

# A revisited study of Cepheids in open clusters in the Gaia era

Gustavo E. Medina,<sup>1\*</sup> Bertrand Lemasle,<sup>1</sup> Eva K. Grebel<sup>1</sup>

<sup>1</sup>*Astronomisches Rechen-Institut, Zentrum für Astronomie der Universität Heidelberg, Mönchhofstr. 12-14, 69120 Heidelberg, Germany*

Accepted XXX. Received YYY; in original form ZZZ

## ABSTRACT

In this paper we revisit the problem of identifying bona fide cluster Cepheids by performing an all-sky search for Cepheids associated with open clusters and making use of state-of-the-art catalogued information for both Cepheids and clusters, based on the unparalleled astrometric precision of the second and early third data releases of the Gaia satellite. We determine membership probabilities by following a Bayesian approach using spatial and kinematic information of the potential cluster-Cepheid pairs. We confirm 19 Cepheid-cluster associations considered in previous studies as bona-fide, and question the established cluster membership of six other associations. In addition, we identify 138 cluster Cepheid candidates of potential interest, mostly in recently discovered open clusters. We report on at least two new clusters possibly hosting more than one Cepheid. Furthermore, we explore the feasibility of using open clusters hosting Cepheids to empirically determine the Cepheid period-age relation through the use of Gaia and 2MASS photometry and a semi-automated method to derive cluster ages. We conclude that the usage of cluster Cepheids as tentative probes of the period-age relations still faces difficulties due to the sparsely populated red giant branch and the stochastically sampled main-sequence turn-off of the open clusters, making age determinations a challenging task. This biases the age-datable cluster selection for Cepheid period-age studies towards older and high-mass clusters.

**Key words:** methods: data analysis – stars: variables: Cepheids – open clusters and associations: general – stars: kinematics and dynamics – catalogues

## 1 INTRODUCTION

Identifying Cepheid variables that are part of stellar associations and open clusters has attracted scientific attention of many astronomers, starting with [Irwin \(1955\)](#), and remains an important research topic. Since they are young objects, Cepheids are expected to be found in stellar associations and young open clusters.

Both Cepheids and young clusters can be used to trace recent star formation events, both in the external galaxies (see e.g., [Payne-Gaposchkin 1974](#); [Efremov 2003](#); [Glatt, Grebel, & Koch 2010](#)), and in the Milky Way, wherein they are expected to trace the spiral arms (e.g., [Magnier et al. 1997a](#); [Pietrzyński et al. 2002](#); [Skowron et al. 2019a](#)). Cepheids are intrinsically rare since the duration of the yellow supergiant stage for intermediate and high mass stars is short, which makes them valuable for constraining models of post-main sequence evolution (e.g., [Bono et al. 2000](#)).

Cepheids in open clusters present several specific interests: first, the clusters can be used as benchmarks for abundance determinations of the Cepheids they host, which are complicated by their pulsating nature (e.g., [Fry & Carney 1997](#); [Lemasle et al. 2017](#)). In addition, the presence of Cepheids in Galactic open clusters has proven to be extremely helpful for the calibration of the Cepheid period-luminosity relation (PLR; see, e.g., [Turner & Burke 2002](#); [Breuval et al. 2020](#)) first found by [Leavitt & Pickering \(1912\)](#), which makes Cepheids cornerstones of the distance scale as it provides a fundamental constraint on the Hubble constant (e.g., [Madore & Freedman 1991](#); [Riess](#)

[et al. 2018](#)). Conversely, the existence of a PLR also allows cluster Cepheids to be used as tools to provide an independent measurement of the distance of the clusters that host them. Finally, in addition to PLRs, theoretical period-age (PA) relations have been established and can be calibrated by studying cluster-Cepheid associations.

Indeed, a longer pulsation period implies a higher stellar mass ([Meyer-Hofmeister 1969](#); [Kippenhahn & Smith 1969](#); [Bono, Castellani, & Marconi 2000](#)) and a younger age for the Cepheid. An empirical PA relation was derived by [Tammann \(1970\)](#) based on Galactic Cepheids and clusters, and later on by [Efremov \(1978\)](#) using Milky Way, M31, and Large Magellanic Cloud clusters. Later, [Magnier et al. \(1997b\)](#) obtained a new semi-empirical relation using Cepheids in the M31 star-forming region NGC 206. Other authors have used larger samples of Cepheids and followed similar approaches to derive PA relations (see, e.g., [Grebel & Brandner 1998](#); [Efremov 2003](#); [Senchyna et al. 2015](#); [Inno et al. 2015](#)). These studies, in addition to recent theoretical approaches ([Bono et al. 2005](#); [Anderson et al. 2016](#); [De Somma et al. 2020b](#)), support the use of PA and PA-colour relations to supply accurate age estimates based only on a few observables.

In spite of their importance, only a small number of bona fide classical Cepheids in open clusters has been reported so far. The available literature illustrates the numerous attempts to increase the list of reliable cluster-Cepheid pairs, starting with the identification of the Cepheids S Nor and U Sgr as members of NGC 6087 and M 25, respectively ([Irwin 1955](#)), and extending throughout the last decades (e.g., [van den Bergh 1957](#); [Kraft 1962](#); [Efremov 1964](#); [Turner 1986](#); [Turner, Forbes, & Pedreros 1992](#); [Turner et al. 1998b](#); [Baumgardt](#)

\* E-mail: [gustavo.medina@uni-heidelberg.de](mailto:gustavo.medina@uni-heidelberg.de)

Dettbarn, & Wielen 2000; Hoyle, Shanks, & Tanvir 2003; Turner et al. 2005; An, Terndrup, & Pinsonneault 2007; Majaess, Turner, & Lane 2008; Turner et al. 2008; Turner 2010; Anderson, Eyer, & Mowlavi 2013; Chen, de Grijs, & Deng 2015; Lohr et al. 2018; Negueruela, Dorda, & Marco 2020). These studies have provided the approximately two tens of currently identified cluster Cepheids. They have faced common obstacles: the scarcity and the inhomogeneity of the input data. In particular, photometry originated from different sources and instruments, and accurate astrometry was rarely available. Spectroscopic information, albeit sparse, was used by several authors when available (e.g., Turner et al. 2008; Anderson, Eyer, & Mowlavi 2013; Usenko et al. 2019).

Large-scale astrometry-focused surveys are required to provide homogeneous catalogues for the study of the Galactic cluster Cepheid populations. The European Space Agency (ESA) mission HIGH Precision PARallax COLlecting Satellite (Hipparcos; ESA 1997) has been an invaluable source of data, allowing the investigation of the association of many Cepheids with open clusters (see, e.g., Lyngå & Lindegren 1998; Turner & Burke 2002). Hipparcos' successor, the ongoing ESA Gaia mission (Gaia Collaboration et al. 2016) revolutionized the study of stellar populations within the Milky Way. Indeed, the second and early third data releases of the Gaia catalogues (hereafter Gaia DR2 and eDR3, respectively) reach limiting magnitudes close to 21 in the  $G$  band with an unparalleled astrometric precision (uncertainties  $< 0.7$  mas for stars brighter than  $G = 20$ ), and include parallaxes and proper motions for more than a billion stars, with photometric precisions at the millimag level (Gaia Collaboration et al. 2018, 2020). In particular, as far as this work is concerned, Gaia has allowed several authors to discover hundreds of new open cluster candidates and to perform membership determinations based on a full astrometric solution of the sources (e.g., Ferreira et al. 2019; Liu & Pang 2019; Torrealba, Belokurov, & Koposov 2019; Cantat-Gaudin et al. 2019; Hunt & Reffert 2021).

With such new data at hand, it becomes possible to update the study of Cepheids in open clusters. In this paper, we describe our investigation of Cepheid cluster membership taking advantage of the large, rich, and homogeneous Gaia data, complemented if needed by other recent surveys. We follow a Bayesian approach based on the method of Anderson, Eyer, & Mowlavi 2013 and using updated literature data. Section 2 describes the data used for our study. In Sections 3 and 4, we describe the Bayesian method used to search for cluster membership, and justify its applicability to the data characterized in Section 2. In Section 5 we report and discuss in detail new cluster Cepheid candidates and compare our results to previous studies. In Section 6 we estimate the age of our sample of cluster Cepheids by age-dating the clusters they are hosted by, and we investigate the feasibility of obtaining an empirical PA relation from our results. Finally, in Section 7 we summarize the contents of our study and describe their implications.

## 2 CEPHEIDS AND OPEN CLUSTERS SAMPLES

To carry out this study, we focused on astrometric and kinematic information for both open clusters and Cepheids.

### 2.1 Open clusters

We rely first on two large public catalogues of known Galactic open clusters: the compilation made by Dias et al. (2002, hereafter D02), for which the last update was published in 2015, and the catalogue

from Kharchenko et al. (2013, hereon K13). The former compilation (D02) consists of 2,167 optically visible clusters and candidates, and is based on the WEBDA database (Mermilliod 1988)<sup>1</sup>, whereas the latter catalogue (K13) contains 3,006 clusters. Combining the clusters from D02 and K13 resulted in a total of 3,135 unique clusters, after removing sources classified as globular clusters by K13. We complemented those with new Milky Way open cluster or open cluster candidates from recent works based on Gaia data:

- from Gaia DR2, Cantat-Gaudin et al. (2018b, hereafter CG18b) and Cantat-Gaudin et al. (2020, henceforth CG20) derived the properties of  $> 1200$  clusters. From these we include 70 and 102 clusters that do not appear in the D02/K13 catalogue, respectively;
- from Gaia DR2, Castro-Ginard et al. (2018) identified 23 nearby open clusters (within 2 kpc from the Sun);
- from Gaia DR2, Castro-Ginard et al. (2019) added 53 new open clusters in the Galactic anticentre and the Perseus arm;
- from Gaia DR2, Cantat-Gaudin et al. (2019, hereafter CG19) added 41 clusters, most of which (33 clusters) located within 2 kpc from the Sun;
- still from Gaia DR2, Ferreira et al. (2019) found three clusters in the field of the intermediate-age cluster NGC 5999, and Ferreira et al. (2020) discovered 25 new open cluster candidates. We added to our sample the 34 open clusters discovered by Ferreira et al. (2021);
- from Gaia DR2, Sim et al. (2019) found 207 open cluster candidates (187 totally new), all located within 1 kpc from the Sun;
- Liu & Pang (2019) identified 76 (mostly old) open cluster candidates (39 totally new) within 4 kpc in the Gaia DR2 data
- the clusters found by Torrealba, Belokurov, & Koposov (2019) using Gaia DR2 were also added, excluding those potentially associated with the Magellanic Clouds (DES 4, DES 5, To 1, and Gaia 3);
- the 582 Galactic disc open clusters recently discovered by Castro-Ginard et al. (2020) using again Gaia DR2 data were also incorporated in our catalogue;
- finally, the 41 recently discovered open cluster candidates detected by Hunt & Reffert (2021) were also included.

We gave priority to the data from D02 over K13. Both were superseded by Gaia DR2 astrometric/kinematic data from the aforementioned studies when available. We checked for duplicated clusters by performing over this compilation an internal cross-match on the cluster center, checking individually all clusters whose centres fell within 3.5 arcmin from each other. After removing evident repeated entries from this list (with astrometric parameters within one standard deviation from each other), our final catalogue contains a total of 4,140 Galactic open clusters. Their spatial distribution is shown in Figure 1.

### 2.2 Cepheids sample

Our catalogue of classical Cepheids relies firstly on the Optical Gravitational Lensing Experiment (OGLE; Udalski, Szymański, & Szymański 2015) database. We compiled the Milky Way classical Cepheids in the disc reported by Udalski et al. (2018) and those in the inner disc towards the Bulge found by Soszyński et al. (2017). We added the additional Cepheids recently added by Soszyński et al. (2020). A number of additional sources list Cepheids, for instance Gaia DR2 (Clementini et al. 2019; Ripepi et al. 2019), the General Catalogue of Variable Stars (GCVS, Kukarkin et al. 1969; Samus' et al. 2017), the Wide-field Infrared Survey Explorer (WISE, Chen

<sup>1</sup> <https://webda.physics.muni.cz>

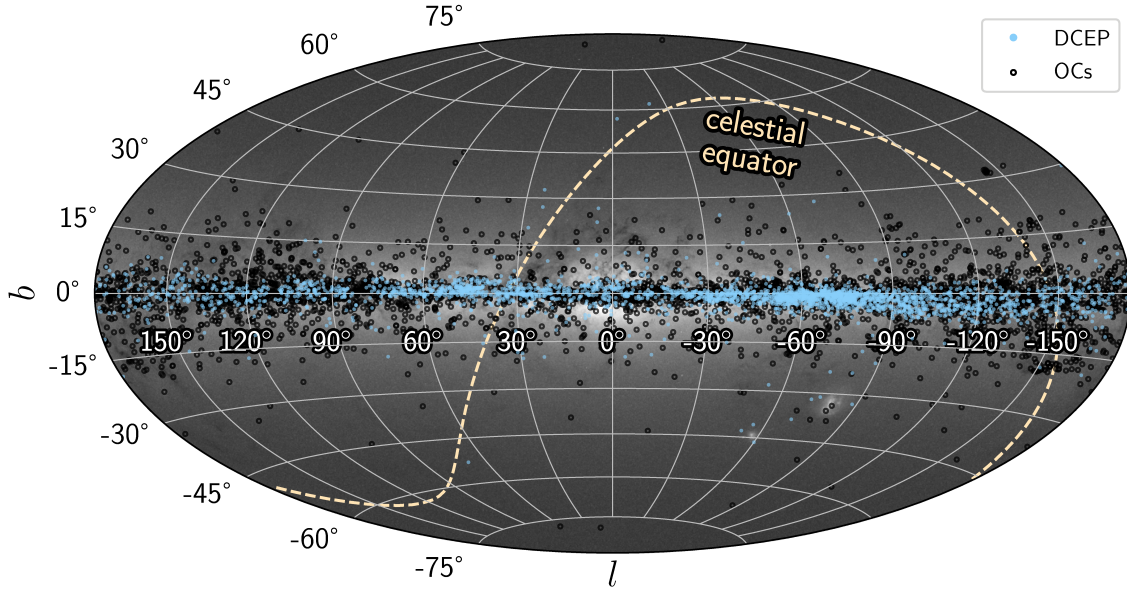


**Figure 1.** Spatial distribution in Galactic coordinates of the Cepheids (DCEP; light blue points) and open clusters (OCs; empty circles) used in this work. The Gaia all-sky map in the background is shown as a reference. *Image Credit: Gaia Data Processing and Analysis Consortium (DPAC); A. Moitinho / A. F. Silva / M. Barros / C. Barata, University of Lisbon, Portugal; H. Saviotto, Fork Research, Portugal.*

et al. 2018), and the Vista Variables in the Vía Láctea survey (VVV, Ferreira Lopes et al. 2020). It is notoriously difficult to classify variable stars in the near- and mid-infrared (light curves become more symmetric and amplitudes decrease, leading to confusion with other types of pulsating variables, eclipsing binaries and spotted stars). The purity of the infrared catalogues is then significantly lower than the purity of the optical ones (Udalski et al. 2018; Dékány et al. 2019). Therefore, we supplemented our catalogue with Cepheids only when they could be detected in the optical as well; hence, we did not include the 640 distant Cepheids recently discovered by Dékány et al. (2019) in the Galactic midplane and bulge. We rely for this on the cross-survey validation performed by the OGLE team, which also includes targets from the Asteroid Terrestrial-impact Last Alert System survey (ATLAS, Heinze et al. 2018) and the All Sky Automated Survey for Supernovae (ASAS-SN, Jayasinghe et al. 2018, 2019a,b) surveys. The Cepheids discovered by Clark et al. (2015) in the cluster BH 222 and by Lohr et al. (2018) in the clusters Berkeley 51 and Berkeley 55 entered our catalogue via this list. The extended catalogue of Cepheids has been used by Skowron et al. (2019a,b) to map the Galactic disc. Once compiled, we cross-matched this catalogue against Gaia eDR3. After removing Cepheids possibly related to the Magellanic Clouds (sources in the region  $254^\circ < l < 324^\circ$ ,  $-54^\circ < b < -22.6^\circ$  with negative parallaxes or with parallax-based distances  $> 10$  kpc), our final sample of Milky Way classical Cepheids contains 2,921 Cepheids with Gaia eDR3 coordinates and proper motions. Their location is indicated in Figure 1.

### 3 MEMBERSHIP DETERMINATION

We follow the Bayesian approach adopted by Anderson, Eyer, & Mowlavi (2013, hereafter A13) to address the membership determination (albeit with differences, which will be detailed in Section 3.3). The Bayesian approach enables us to quantify the likelihood of a given Cepheid being a member of an open cluster. We refer to a

Cepheid-cluster pair as a “combo”, following the convention initiated by A13. To determine the membership probabilities, we use positional and kinematic constraints on both Cepheids and clusters: projected on-sky distances, parallaxes, proper motions, and radial velocities (RV) where available.

Using Bayes’ theorem (see, e.g., Jaynes 2003), the posterior  $P(A|B)$ , i.e., the membership probability, is computed from:

$$P(A|B) \propto P(B|A) \times P(A) \quad (1)$$

where  $P(B|A)$  is the conditional probability of obtaining the cluster and Cepheid data assuming that their association is real (the likelihood), and  $P(A)$  (the prior) represents the probability distribution that expresses our belief of membership before the evidence used for  $P(B|A)$  is considered. We emphasize that this methodology relies on a hypothesis test that assumes membership. Thus, the association between a Cepheid and a cluster cannot be proven but only refuted by following this approach.

In Equation 1, a normalization term associated with the probability of observing the data is neglected, given that we possess no knowledge to quantify it. In the rest of this subsection, we detail the procedure and assumptions on which the determination of the probabilities  $P(B|A)$  and  $P(A)$  are based.

#### 3.1 On-Sky Selection and Prior $P(A)$

As other works have done in the past, we perform an initial cross-match based on the on-sky position of Cepheids and open clusters, taking into account the actual size of the clusters. The goal is to identify possible combos and to rule out Cepheids easily recognizable as non-members. This also reduces the computation time of the next steps of our analysis.

To achieve this, we first estimate the apparent size of each cluster. K13 provide a list of cluster size parameters denoted as  $r_0$ ,  $r_1$ , and  $r_2$ , which represent the angular radius of the core, the central part, and the entire cluster, respectively. They were fitted by eye to describe



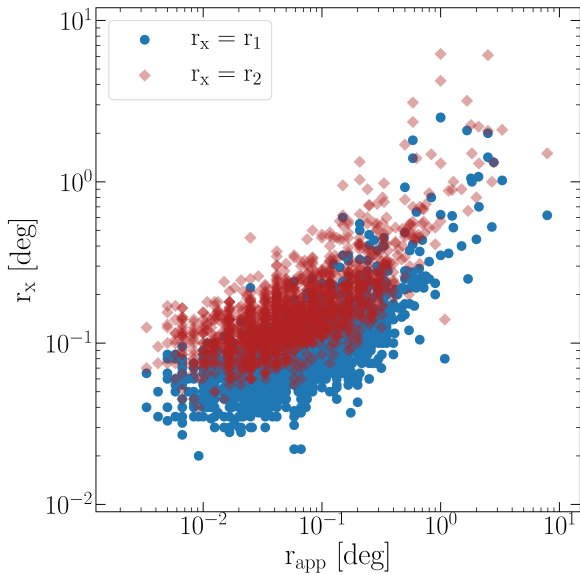


**Figure 2.** Correlation between the open cluster apparent radii listed in D02 and the radii  $r_1$  and  $r_2$  presented by K13, plotted with blue dots and red diamonds, respectively.

the shape of the clusters radial density profiles (Kharchenko et al. 2012). Clusters from sources other than K13 do not provide these particular parameters as estimators of the cluster sizes. However, A13 demonstrated that  $r_1$  and  $r_2$  given by Kharchenko et al. (2012) are correlated with the core and limiting radius of the clusters provided by Kharchenko et al. (2005a) and Kharchenko et al. (2005b), respectively. Then, A13 used the trend between the core and limiting radii and the values from D02 to finally get an estimate of these clusters' sizes. In the case of clusters that are only present in D02, they do have an estimation of their sizes, but in the form of an angular apparent diameter. Unsurprisingly, we found correlations between the apparent radius,  $r_{\text{app}}$ , and  $r_1$  and  $r_2$  (as seen in Figure 2), but they show considerable scatter. The correlations are:

$$\begin{aligned} r_1 &= 0.3037 \cdot r_{\text{app}} + 0.0688, \\ r_2 &= 0.6060 \cdot r_{\text{app}} + 0.1252, \end{aligned} \quad (2)$$

which we used to estimate  $r_1$  and  $r_2$  for this subsample of clusters.

In CG18b, CG19, and CG20, the authors present the value  $r_{50}$ , which represents the radius containing half the members. For these clusters, we assumed  $r_1 = r_{50}$ , and  $r_2 = r_1 \cdot 1.957$ , where the scaling factor is the ratio between  $r_2$  and  $r_1$  in K13, and their correlation factor is 0.962. We made the same assumptions for the clusters from Hunt & Reffert (2021), for which  $r_{50}$  is provided. In a recent work, Sánchez, Alfaro, & López-Martínez (2020) determined the radii of a sub-sample of open clusters available in the literature based on Gaia DR2 proper motions. As a comparison, the median difference between the clusters'  $r_{50}$  in CG20 and the cluster radii from Sánchez, Alfaro, & López-Martínez (2020) is 1.19 pc for the 357 clusters in common.

For the clusters provided by Ferreira et al. (2019, 2020), we use directly the values given in their work, as they provide estimations for both the core radius and the limiting radius. We assumed those values to be good representations of  $r_1$  and  $r_2$ , respectively. Ferreira et al. (2021) provide only an estimation of the clusters limiting radius  $r_{\text{lim}}$ . Thus, for those clusters we assumed  $r_2 = r_{\text{lim}}$ , and  $r_1 = r_2/1.957$ . Regarding the nine clusters from Torrealba, Belokurov, & Koposov

(2019), the authors provide a direct estimation of the half-light radius ( $r_h$ ). In order to obtain  $r_1$  and  $r_2$ , we assume  $r_1 = r_h$ , and applied the scaling factor 1.957 to estimate  $r_2$ .

The case of the clusters discovered by Liu & Pang (2019) and Sim et al. (2019) is similar. The catalogue published by Liu & Pang (2019) provides the distance of the furthest member to the average member position as a proxy of the clusters' size,  $r_{\text{MAX}}$ . We considered  $r_2 = r_{\text{MAX}}$  in those cases. The catalogue that characterizes the cluster candidates found by Sim et al. (2019) gives the core radius as an estimation of the clusters size. We adopted those values as the clusters'  $r_1$ . For both the Liu & Pang (2019) and the Sim et al. (2019) clusters, we again assumed the values of  $r_2$  to be about twice as large as  $r_1$ .

For the clusters from the works by Castro-Ginard et al. (2018, 2019, 2020), a list of tentative cluster members was also published by the authors. With this information we computed the radii  $r_1$  and  $r_2$  using the previously mentioned scaling factor and setting  $r_1 = r_{50}$ , the median cluster member distance (as provided by Castro-Ginard et al. 2018, 2019, 2020) with respect to their tabulated central coordinates.

With an estimated cluster size, it is possible to perform the initial cross-match based on the on-sky position of the Cepheid-open cluster pairs. To minimize the list of possible combinations for which we compute probabilities, we selected all Cepheids within the largest distance between 2 deg from a given cluster centre, or five times the cluster's  $r_1$ . This is similar to the procedure followed by A13. With the median  $r_1$  of the entire sample at 0.08 deg and with  $\sim 95$  per cent of the clusters having values of  $r_1 < 0.4$  deg, we consider that finding a Cepheid at more than 2 deg from the cluster centre makes its membership unlikely and justifies such an arbitrary choice. For the remaining clusters, for which the median  $r_1$  is 0.6 deg, choosing the limit at  $5 \cdot r_1$  allows for some flexibility, even when computing probabilities for nearby associations with  $r_1 > 1$  deg, such as Collinder 285.

A total of  $\sim 44,300$  possible combos results from this procedure. We focus on these combinations in the next steps of our membership analysis, starting with the determination of the prior.

We define the prior  $P(A)$  following A13's approach: we only take into account the on-sky separation between a Cepheid and a cluster, and the apparent size of the latter based on its core and limiting radius. By defining the quantity  $x$  as:

$$x = \frac{r - r_1}{2 \cdot r_2 - r_1} \quad (3)$$

where  $r$  is the on-sky separation,  $r_1$  is a proxy for the core radius, and  $r_2$  a proxy for the limiting radius, we can measure the relative position of the Cepheid with respect to the centre of the cluster, weighted by its size. Then, for the value of the probability we define:

$$\begin{aligned} P(A) &\equiv 1, & x < 0 \\ P(A) &\equiv 10^{-x}, & x \geq 0 \end{aligned} \quad (4)$$

From this definition, a combo's prior probability will be 1 if the Cepheid falls within the core of the cluster, and will reach 10 per cent at  $x = 1$ , inspired by the exponential decline of the radial profile of star clusters. We note that in the study by A13 the authors define the prior such that it reaches 0.1 per cent at  $x = 1$ . Considering only the prior, this means that we are more flexible than A13 when computing probabilities.

We modified the prior with respect to A13 to take into account



the recent results of e.g., Meingast, Alves, & Rottensteiner (2021): from a sample of young open clusters with ages between 30 and 300 Myr (perfectly matching the ages of Cepheids), they found that almost all clusters are surrounded by a large halo of stars they call coronae and which extend further than 100 pc from the clusters' centre. Most clusters show evidences of expansion along one or more spatial axes, a feature also observed by, e.g., Pang et al. (2020). Although reminiscent of tidal features observed in older clusters, such features are most likely primordial and related to filamentary star formation (e.g., Beccari, Boffin, & Jerabkova 2020; Tian 2020). With a somewhat relaxed prior, we are more likely to recover bona-fide cluster Cepheids located at large distances from the cluster centre, but also more exposed to spurious detections. We note in passing that for a Cepheid located at  $5 \cdot r_1$  from the centre of a cluster (one of the pre-selection criteria adopted above), Equation 4 would return  $P(A) \approx 0.05$  when  $r_2 \approx 2 \cdot r_1$ .

### 3.2 The Likelihood $P(B|A)$

As other authors have done in the past (Robichon et al. 1999; Baumgardt, Dettbarn, & Wielen 2000; A13; Hanke et al. 2020; Prudil et al. 2021), we determine the likelihood of membership  $P(B|A)$  as a hypothesis test based on the Mahalanobis distance (introduced by Mahalanobis 1936), which is a measure of the distance between a point (a Cepheid) and a distribution (an open cluster). The task of calculating quantiles for multivariate normal distributions is not as simple as in the one-dimensional case, since these quantiles can be considered ellipsoids in dimensions higher than two. However, calculating the Mahalanobis distance is a rather simple method to describe all points on the surface of such a multidimensional ellipsoid.

Given a vector  $z$  built as the difference  $\Delta$  between the Cepheid and the mean cluster parameters (here we consider the parallaxes  $\varpi$ , proper motion in right ascension  $\mu_\alpha^*$  and declination  $\mu_\delta$ , and the radial velocities  $V_r$ ):

$$\vec{z} = (\Delta\varpi, \Delta\mu_\alpha^*, \Delta\mu_\delta, \Delta V_r) \quad (5)$$

the square of the Mahalanobis distance between the Cepheid and the cluster,  $c$ , can be expressed as:

$$c = \vec{z}^T \Sigma^{-1} \vec{z}, \quad (6)$$

where  $\vec{z}^T$  is the transpose of  $\vec{z}$ , and  $\Sigma^{-1}$  denotes the inverse of the sum of the covariance matrices of a cluster and a Cepheid when systematic effects and correlations are taken into account. It should be noted that, for the purpose of these calculations, we compute  $c$  under the assumption that the Cepheid was not used to measure the mean cluster parameters.

An additional quantity that we used to determine  $\Sigma^{-1}$  is the re-normalized unit weight error (RUWE), which is given as a parameter in the Gaia DR2 and eDR3 catalogues and which accounts for the fitting effects when the astrometric solution is poor (Lindegren et al. 2018). For sources where the Gaia single-star model is well fitted, the RUWE is expected to be close to 1.0, and values significantly greater than 1.0 reflect problems in the astrometric solution or non-single objects. To account for this, for stars with  $\text{RUWE} > 1.4$  we scaled the elements of the covariance matrix that are taken from the Gaia catalogues by the square of their RUWE values. If a given Cepheid has a non-numerical RUWE, we set its value to 22, which corresponds to the maximum value of the original list of Cepheids in the Gaia catalogue.

We assume the clusters' covariance matrices to be diagonal whenever the data collected come from several sources, and we possess no information about possible correlations. If correlations between

the cluster parameters are known and given in the cluster sources or can be inferred from, for example, Gaia data, the mean values from the clusters members are included in the corresponding cluster's covariance matrix. For the Cepheids' matrices we used the correlations between parallaxes and proper motions explicitly provided by the Gaia eDR3 catalogue. Finally, we assume the correlation between the properties of clusters and Cepheids to be negligible.

It is possible to show that, under these conditions, and assuming Gaussian distributions, the Mahalanobis distance  $c$  is actually  $\chi^2$ -distributed. It is worth mentioning that the shape of the  $\chi^2$  distribution depends on the number of dimensions of  $\vec{z}$ , i.e., the number of constraints considered for the combo. Finally, the likelihood is the result of:

$$P(B|A) = 1 - p(c) \quad (7)$$

where  $p(c)$  represents the probability of finding a value at least as extreme as the observed  $c$  under the null hypothesis of (true) membership, that is, is the p-value of  $c$ .

### 3.3 Differences with A13

Although our study follows the Bayesian approach of A13, there are also significant differences, both in the method and in the data, since we benefit from greatly improved data quality thanks to Gaia in particular. We discuss these differences here below:

A13 initially considered 2,168 clusters. In our study, many more entered the catalogue, since the D02 database has been continuously updated and thanks to the discovery of numerous open clusters after Gaia DR2. Our catalogue contains over 4,000 clusters. Moreover, cluster parallaxes and proper motions have been updated to Gaia DR2 values for roughly half of our cluster catalogue.

Our initial catalogue of Cepheids is also much larger than the one used in A13 (2,921 vs. 1,821) thanks to numerous surveys having provided a large number of new Cepheids. Parallaxes in A13 are taken directly from the Hubble Space Telescope (8 stars, Benedict et al. 2007), from the study by Storm et al. (2011) for 33 stars, and from Hipparcos (van Leeuwen 2007) for a good fraction of their sample. For 622 Cepheids, parallaxes are derived by inverting the distance to the Cepheid, computed using a period-luminosity relation in the V-band since the largest photometric data sets are available in this band. Although computed with the greatest care, this method suffers from the intrinsic width of the instability strip, which is much larger than in the near-infrared for instance, from the metallicity dependence of V-band period-luminosity relations (e.g., Romaniello et al. 2008), from the heterogeneity of the photometric data sets used, and from very large uncertainties on the adopted values for  $E(B-V)$ . We benefit instead from the great quality of Gaia eDR3 parallaxes. Finally, the proper motions for Cepheids in A13 are taken from Hipparcos (van Leeuwen 2007) when available and from the Position and Proper Motion Extended-L catalogue (PPMXL; Roeser, Demleitner, & Schilbach 2010) otherwise, while ours are also from Gaia eDR3. Radial velocities are comparable in terms of data availability, accuracy, and precision.

In Figure 3, we compare the astrometric and kinematic data sets, after cross-matching the  $\sim 4,000$  pairs investigated by A13 against our  $\sim 44,300$  candidates. Since no other comparison data are available, we compare the difference between a given Cepheid and its potential host in both data sets. On the other hand, such a comparison relates directly to possible differences in the probabilities  $P(B|A)$  derived by each study. We note that even small discrepancies may be significant in the computation of  $P(B|A)$ . In terms of proper motions, the spreads

of the distributions are of the order of tens of  $\text{mas yr}^{-1}$ , and can be as high as  $\sim 180 \text{ mas yr}^{-1}$ .

We mentioned earlier that we adopted a different prior for cluster membership, to take into account the mounting evidence of large spatial extensions even for young clusters. Since this particular property had not been discovered yet, A13 adopted a stricter prior that is less sensitive to the clusters' outskirts but conversely less prone to false positives. We note in passing that an even looser prior has been used by [Hanke et al. \(2020\)](#) in a search for extra-tidal halo stars in the neighborhood of globular clusters.

Another important difference is that, in contrast to A13, who took into account up to six dimensions when computing the square of the Mahalanobis distance, we only consider up to four ( $\varpi$ ,  $\mu_\alpha^*$ ,  $\mu_\delta$ , and  $V_r$ ), and neither ages nor metallicities, in the computation of  $c$ .

If we were to include ages in our analysis, we would necessarily have computed the Cepheids' ages from period-age relations. This is, however, impossible in our case since one of our goals is to constrain such relations. Moreover, ages derived from period-age relations with an average stellar rotation ( $\Omega_{\text{ZAMS}}/\Omega_{\text{crit}} = 0.5$ , [Anderson et al. 2016](#)) are 50-100 per cent higher than those derived from period-age relations without rotation (e.g., [Bono et al. 2005](#)). As far as clusters are concerned, for 93 per cent of the clusters in D02 ages were provided. From the numerous clusters discovered in Gaia DR2 data, a good fraction has ages available ([Bossini et al. 2019](#), CG20, without quoted uncertainties for the vast majority). However, the difficulty to properly identify the main-sequence turnoff (MSTO) compromises the age determination via the isochrone-fitting method for young clusters, that is, those potentially hosting Cepheids, especially when using an automated algorithm as we experienced ourselves (see Section 6 for a more detailed discussion). The difficulty is reduced towards higher ages, when the MSTO and the red giant branch (RGB) become more populated, and A13 allowed for varying uncertainties in age to take this effect into account. As pointed out by A13, even large uncertainties are useful, in the sense that they allow us to filter out pairs for which ages definitely mismatch. Our concern here is that pairs could be rejected on the basis of an inaccurate age determination, even when allowing for large uncertainties.

The situation is even worse in the case of the metallicity, since  $[\text{Fe}/\text{H}]$  is available only for a small fraction of the clusters, and often relies on disparate techniques (photometric estimates, low-resolution spectroscopy, high-resolution spectroscopy) and very few cluster members. Many have attempted to provide homogeneous metallicity scales in the recent past, either within a given large spectroscopic survey or by collecting data from various sources (e.g., [Netopil et al. 2016](#)), but the number of clusters with available metallicities falling in the age range considered here is very small. Studies of the Milky Way radial abundance gradient indicate a good agreement between  $< 1$  Gyr old open clusters and Cepheids, both for  $[\text{Fe}/\text{H}]$  and other elements (e.g., [Lemasle et al. 2008](#); [Genovali et al. 2015](#); [Magrini et al. 2017](#)), but detailed comparisons are still missing. [Fry & Carney \(1997\)](#) found a good agreement ( $\approx 0.1$  dex) between the metallicity of two main-sequence stars and the Cepheid U Sgr in M25, but the comparison is limited to  $[\text{Fe}/\text{H}]$ . [Lemasle et al. \(2017\)](#) found a similarly good agreement between 6 Cepheids and a large number of RGB stars analyzed by [Mucciarelli et al. \(2011\)](#) in the young LMC cluster NGC 1866, which contains 24 Cepheids ([Musella et al. 2016](#)) and is therefore not representative of Milky Way young clusters.

On the basis of the above, we decided to search for possible cluster-Cepheid combos relying on astrometry and kinematics only, awaiting for a membership confirmation from studies including a detailed age and chemical analysis.

## 4 THE DATA

### 4.1 Parallaxes

For the open clusters in our list (see Section 2) we used the parallaxes and their associated uncertainties directly from their original sources, if available. If not (as for the D02 clusters), we derived the parallaxes  $\varpi$  from the published distances  $d$  in parsecs, following:

$$\begin{aligned}\varpi &= \frac{1000}{d} \text{ (mas)}, \\ \sigma_\varpi &= \frac{1000}{d^2} \cdot \sigma_d \text{ (mas)},\end{aligned}\tag{8}$$

where  $\sigma_d$  represents the distance uncertainty, and  $\sigma_\varpi$  the corresponding assumed parallax uncertainty. We consider this approximation justified since there is an overall good agreement between parallaxes computed this way and those provided by CG20 using Gaia DR2 data with a median difference of 0.08 mas for the clusters in common between that study and D02. In such a case we enforced a distance uncertainty of 20 per cent (as done by A13) to account for various effects impacting the distance determination such as stellar rotation and binarity.

In any case, older values are superseded by parallaxes and parallax errors from Gaia DR2 when available. Moreover, [Lindegren et al. \(2018\)](#) reported a (global) zero-point shift of  $-0.03$  mas for Gaia DR2 parallaxes. Unless this was explicitly accounted for in the original papers, we shifted the Gaia DR2 parallaxes accordingly.

In addition, parallaxes of Gaia sources located close to each other on the sky are highly correlated, especially when they are separated by less than one degree. Following the recommendations of [Lindegren et al. \(2018\)](#) for sources separated by an angle  $\theta$ , we computed the mean spatial covariance of the parallax errors  $V_\varpi(\theta)$  of the members of each cluster in our sample based on Gaia DR2 data, if a list of members was available in the source catalogue, and if these spatial covariances were not originally considered. Otherwise, spatial covariances were neglected. The corresponding systematic uncertainties and additional correlations are then included in the covariance matrices of the clusters.

For the Cepheids, parallaxes from Gaia eDR3 are available for all the stars in our sample. We corrected them for the Gaia eDR3 zero-point parallax offset following [Lindegren et al. \(2020\)](#)<sup>2</sup>, and we increased the uncertainties by 10 per cent to account for their likely underestimation, based on the work of [Fabricius et al. \(2020\)](#). As in the case of the clusters, these changes were included in the covariance matrices of the Cepheids.

### 4.2 Proper Motions

The (mean) proper motions in right ascension and declination and their respective uncertainties were first taken from D02. Some clusters are registered only in K13, where a single value  $\sigma_\mu$  is given for the proper motion uncertainties. We therefore adopted  $\sigma_{\mu_\alpha}^* = \sigma_{\mu_\delta} = \sigma_\mu/\sqrt{2}$ . These values were replaced by proper motions based on Gaia DR2 when available. In this case, we adopted the values tabulated in the respective source catalogues for the proper motions and their uncertainties.

Similarly to the  $V_\varpi(\theta)$  correction described above, we corrected the Gaia DR2 proper motion uncertainties by taking into account the spatial covariances  $V_\mu(\theta)$  that affect sources located close to each other in the sky ([Lindegren et al. 2018](#)), in this case the members of

<sup>2</sup> [https://gitlab.com/icc-ub/public/gaiadr3\\_zero\\_point](https://gitlab.com/icc-ub/public/gaiadr3_zero_point)

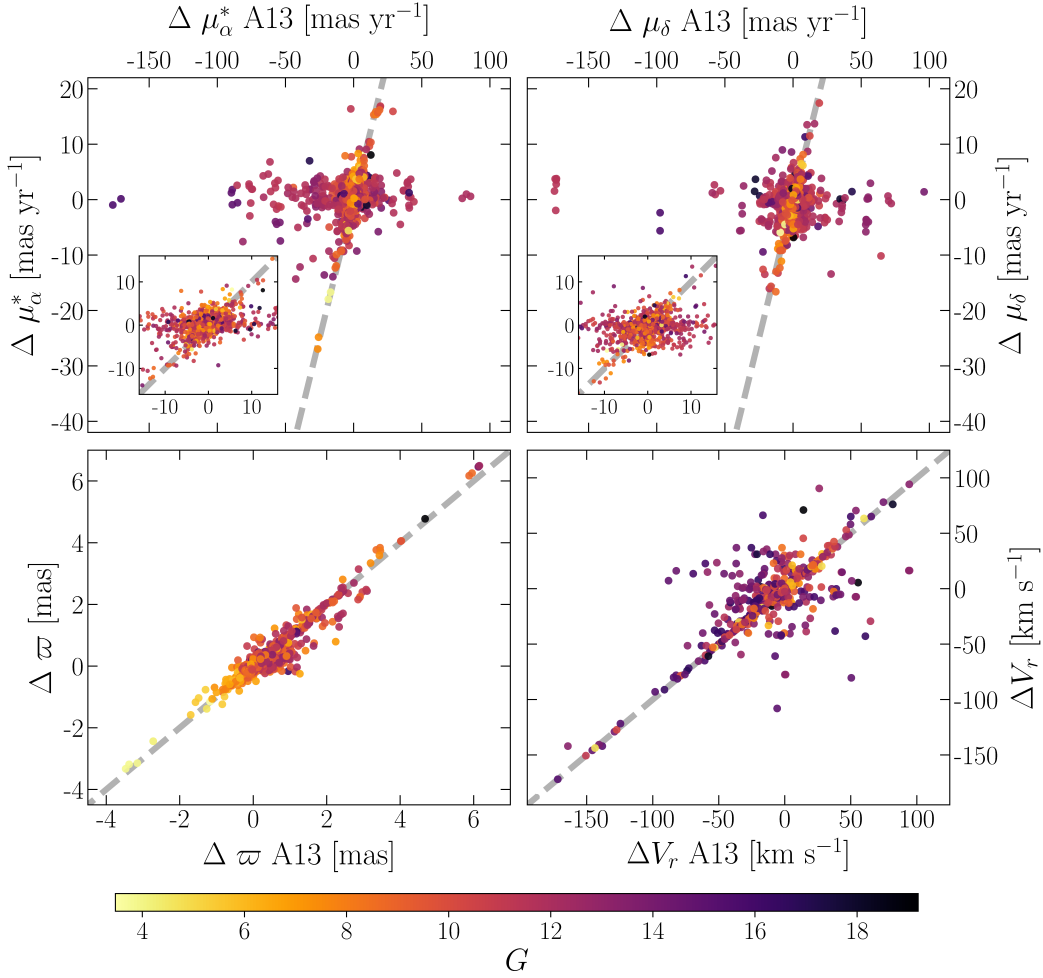


**Figure 3.** Comparison of the differences in proper motions, parallaxes, and radial velocities between clusters and Cepheids for the combos in common with A13. The filled circles shown are colour-coded by the Cepheids’ mean  $G$  magnitudes. A grey dashed line representing the identity function is plotted in each panel as a reference. In the plots displaying proper motion differences (*upper panels*) we include an enlargement of the central distribution of points.

a given cluster, and added the mean  $V_{\mu}(\theta)$  of such a cluster as a systematic uncertainty when this effect was not already accounted for in the original studies. For the clusters with Gaia DR2 proper motions but no list of members (which have sizes as small as  $\sim 0.01$  deg), we added a systematic uncertainty of  $0.066 \text{ mas yr}^{-1}$  following the recommendations of Vasiliev (2019) (see their Figure 3). These changes were propagated in the cluster covariance matrices.

In the case of the Cepheids, we take their proper motions directly from the Gaia eDR3 catalogue. We revised these values using the Gaia eDR3 proper motion bias correction recently described by Cantat-Gaudin & Brandt (2021), and added a systematic error of  $-10 \mu\text{as yr}^{-1}$  to the uncertainties of the Cepheids with  $G < 13$  listed in the catalogue to account for the remaining color-dependent systematics discussed by these authors. These changes were included in the covariance matrices of the Cepheids.

### 4.3 Radial Velocities

For the radial velocity of the open clusters, we use the mean values and uncertainties listed in D02. We note, however, that for a given cluster, the uncertainty on the radial velocity provides a good estimate of the intrinsic velocity dispersion only when the number of

stars analyzed is large. For clusters only present in K13, where no uncertainty is given, we follow A13’s reasoning and estimate this value by computing  $\sigma_{ocRV} = 10/\sqrt{N_{RV}} \text{ km s}^{-1}$ , where  $N_{RV}$  is the number of stars used to compute the radial velocity of the cluster. If  $N_{RV}$  is also missing, we assume a value of  $15 \text{ km s}^{-1}$ , which matches the maximum velocity dispersion for open clusters recently analyzed by, e.g., Carrera et al. (2019) and Donor et al. (2020).

To update the radial velocities and associated uncertainties of our cluster catalogue we used the information of 131 clusters listed in Carrera et al. (2019), obtained by data mining the Apache Point Observatory Galactic Evolution Experiment (APOGEE DR14, Abolfathi et al. 2018; Holtzman et al. 2018) and the Galactic Archaeology with HERMES survey (GALAH DR2, Buder et al. 2018). Of these open clusters, 127 are in common with the original D02 + K13 catalogues, of which 72 have previously derived radial velocities (in D02 + K13). We also considered the radial velocities of the 128 clusters listed in Donor et al. (2020), who examined APOGEE data (DR16, Jönsson et al. 2020). Of these clusters, 126 are listed in the catalogue of D02 and K13. We note that the mean absolute radial velocity difference between the values listed in the D02 and K13 catalogues, and those catalogued by Carrera et al. (2019) and Donor et al. (2020) is  $12.1 \pm 26.1 \text{ km s}^{-1}$  and  $7.5 \pm 13.9 \text{ km s}^{-1}$ , respectively. For the



clusters for which more than one radial velocity measurement is available, we give priority to the more recent studies over older ones (including those in D02 and K13, since we favour the homogeneity of the data). In any case, we impose a minimum velocity dispersion of  $2 \text{ km s}^{-1}$ , a value also in line with the compilations of [Carrera et al. \(2019\)](#) and [Donor et al. \(2020\)](#) for clusters in which the measured velocity dispersion relies on more than 10 stars.

As classical Cepheids are pulsating stars, monitoring observations are required to derive their systemic velocity (or alternatively radial velocity templates). Such data are in general not available, and we rely on the compilation made by [Mel'nik et al. \(2015\)](#), in which they provide heliocentric radial velocities and their uncertainties for  $\sim 320$  Cepheids from different sources (see references in [Mel'nik et al. 2015](#)). To take into account possible phase coverage biases or binarity (up to 80 per cent of Cepheids are in binary systems, [Kervella et al. 2019](#)), we impose an arbitrary minimum uncertainty for the Cepheids' radial velocities of  $2 \text{ km s}^{-1}$ .

## 5 MEMBERSHIP DETERMINATION: THE OUTCOME

Of the total  $\sim 44,300$  possible combos for which we computed the likelihood of membership, only a small fraction displays relatively high probabilities, and the sample is strongly dominated by cluster-Cepheid pairs with probabilities  $\leq 10^{-5}$ . From the cluster-Cepheid pairs with higher membership probabilities, 163 have probabilities higher than 1 per cent, 67 have probabilities over 10 per cent, and only 44 over 25 per cent. The thresholds mentioned here are only meant to give an overview of the results and bear no implication on membership, as our methodology relies on a hypothesis test that assumes membership in the first place. Cluster-Cepheid pairs with posterior probabilities higher than 0.10 are shown in Table 1. Those with membership probabilities from 0.01 to 0.10 can be found in the appendix (Table A1).

In Section 5.1 we briefly discuss a few combos from the literature that we consider recovered, relying mostly on the cluster Cepheid catalogues from David Turner<sup>3</sup>, A13, and [Chen, de Grijs, & Deng \(2015\)](#). In Section 5.2, we briefly discuss six combos reported in at least three previous studies (from the aforementioned ones plus [Röck 2012](#)) for which we obtain marginal membership probabilities. In Table A2 we show the results of these comparisons with literature combos. In Section 5.4 we discuss a few arbitrarily selected combos.

### 5.1 A few bona fide combos from the literature

#### 5.1.1 The Cepheids around NGC 7790

We recover the three Cepheids CE Cas A, and CE Cas B, CF Cas paired to the cluster NGC 7790 (widely known as the only Galactic open cluster hosting three Cepheids), with relatively high association probabilities. The three Cepheids are bright ( $G \sim 10$  mag) fundamental-mode pulsators with similar periods of  $\sim 5$  d ([Ripepi et al. 2019](#)), indicating they have a similar age.

Our algorithm also reports a non-negligible probability of association of these three Cepheids with LP 888 ([Liu & Pang 2019](#), even with a slightly larger probability for CE Cas A) or with UBC 404. Although they are close to each other in the vicinity of NGC 7790, LP 888 and UBC 404 are reported as different structures by [Liu & Pang \(2019\)](#) and [Castro-Ginard et al. \(2020\)](#), respectively. From previous knowledge (e.g., [Sandage 1958](#); [Mateo & Madore 1988](#);

[Matthews et al. 1995](#); [Majaess et al. 2013b](#)) and given  $P(A)=1$ , the three Cepheids are clearly members of NGC 7790, but the quite high likelihoods computed suggest a dynamical association between NGC 7790 and the other structures newly discovered nearby.

#### 5.1.2 The Cepheids in NGC 6067

A second case of well-known cluster-Cepheid associations are the Cepheids V0340 Nor and QZ Nor and the cluster NGC 6067. An extensive discussion addressing the possible membership of, especially, QZ Nor is available in the literature (see e.g., [Eggen 1980](#); [Walker 1985b](#); [Coulson & Caldwell 1985](#); [An, Terndrup, & Pinsonneault 2007](#); [Turner 2010](#); [Majaess, Turner, & Lane 2008](#)). A dedicated study performed by [Majaess et al. \(2013a\)](#) confirmed both stars as members of NGC 6067. Recently, [Breuval et al. \(2020\)](#) interpreted the proper motion difference between the cluster and QZ Nor as a hint that the Cepheid is leaving the cluster. The striking difference in the membership probability (66 per cent for V0340 Nor versus  $< 1$  per cent for QZ Nor) is a strong indication that the dynamical state of the cluster can have a strong impact on the membership probability. This is the reason why we provide a list of potential combos with a low membership probability, ranging from 1 to 10 per cent (Table A1) as it may contain similar cases. Finally, [Breuval et al. \(2020\)](#) proposes GU Nor as a potential member of NGC 6067 as well. We find a posterior probability  $< 0.01$  for this pair, as both its prior and likelihood are not significant.

#### 5.1.3 GQ Vul and FSR 0158

For the combo consisting of the distant open cluster FSR 0158 ([Froeblich, Scholz, & Raftery 2007](#)) and the Cepheid GQ Vul we also obtain a high association probability (0.47). This result is a combination of the position of the Cepheid close to the cluster's centre and the excellent agreement between their proper motions and parallaxes. It had been reported so far only by A13 with a probability of 43 per cent. We note, however, a discrepancy between the distance of FSR 0158 according to CG20 ( $\sim 6, 100$  pc) and the distance of GQ Vul ( $\sim 4, 500$  pc) derived by [Wang et al. \(2018\)](#) using a PL relation in the mid-infrared. Similarly, GQ Vul is about  $\sim 35$  Myr old from the theoretical PA relation of [Bono et al. \(2005\)](#), whereas the cluster age as determined by CG20 is  $< 10$  Myr, a value incompatible with the presence of a Cepheid. However, it is noteworthy that only 27 stars are considered as cluster members with a probability higher than 50 per cent, and only 14 with probabilities higher than 70 per cent (CG18b, CG20), which may significantly affect the determination of FSR 0158's distance and age.

Combos for which we obtain  $P(A|B) > 0.01$  and that appear at least once in Turner's database, A13 (with membership probability  $> 0.10$  from their work), or [Chen, de Grijs, & Deng \(2015\)](#), together with the spectroscopically confirmed cluster Cepheids described by [Lohr et al. \(2018\)](#) and [Clark et al. \(2015\)](#), and the association recently found by [Negueruela, Dorda, & Marco \(2020\)](#), are listed at the top of Table A2 (19 in total).

### 5.2 Missed combos from the literature

Beyond the fact that combos previously reported in the literature might simply be discarded in the light of new, more accurate data, we could be unable to recover real combos for several reasons:

We exclude the fact that a cluster, and especially a Cepheid are

<sup>3</sup> <http://www.ap.smu.ca/~turner/cdlist.html>

**Table 1.** Cluster - Cepheid pairs with membership probabilities  $P(A|B) > 0.10$ . The table lists the cluster names as well as their MWSC identification in the K13 catalogue, the Cepheid names, the ratio between the separation of the pair and the cluster's  $r_1$  (Sep/ $r_1$ ), the list of constraints used to derive the membership probability, the prior  $P(A)$ , the likelihood  $P(B|A)$  and the membership probability  $P(A|B)$ .

Open cluster	MWSC ID	Cepheid	Sep/ $r_1$	Constraints	$P(A)$	$P(B A)$	$P(A B)$
Trumpler 14	1846	OGLE-GD-CEP-1673	0.57	$\varpi, \mu_{\alpha}^*, \mu_{\delta}$	1.00	1.00	1.00
UBC 553	–	OGLE-GD-CEP-1194	0.54	$\varpi, \mu_{\alpha}^*, \mu_{\delta}$	1.00	0.99	0.99
Berkeley 55	3490	ASASSN-V J211659.90+514558.7	0.29	$\varpi, \mu_{\alpha}^*, \mu_{\delta}$	1.00	0.94	0.94
Gaia 5	–	V0423 CMa	0.81	$\varpi$	1.00	0.94	0.94
ASCC 79	2288	OGLE-GD-CEP-1752*	0.78	$\varpi, \mu_{\alpha}^*, \mu_{\delta}$	1.00	0.94	0.94
Berkeley 51	3280	ASASSN-V J201151.18+342447.2	0.75	$\varpi, \mu_{\alpha}^*, \mu_{\delta}$	1.00	0.85	0.85
Harvard 16	2616	OGLE-BLG-CEP-041	0.75	$\varpi, \mu_{\alpha}^*, \mu_{\delta}$	1.00	0.83	0.83
FSR 0951	849	RS Ori	0.24	$\varpi, V_r, \mu_{\alpha}^*, \mu_{\delta}$	1.00	0.82	0.82
Lynga 6	2348	TW Nor	0.39	$\varpi, V_r, \mu_{\alpha}^*, \mu_{\delta}$	1.00	0.82	0.82
NGC 7790	3781	CF Cas	0.30	$\varpi, V_r, \mu_{\alpha}^*, \mu_{\delta}$	1.00	0.80	0.80
Gulliver 9	–	AM Vel	1.33	$\varpi, \mu_{\alpha}^*, \mu_{\delta}$	0.77	1.00	0.77
IC 4725	2940	U Sgr	0.10	$\varpi, V_r, \mu_{\alpha}^*, \mu_{\delta}$	1.00	0.75	0.75
NGC 129	53	DL Cas	0.04	$\varpi, V_r, \mu_{\alpha}^*, \mu_{\delta}$	1.00	0.75	0.75
Czernik 41	3192	J297.7863+25.3136	0.65	$\varpi, \mu_{\alpha}^*, \mu_{\delta}$	1.00	0.73	0.73
vdBergh 1	934	CV Mon	0.68	$\varpi, \mu_{\alpha}^*, \mu_{\delta}$	1.00	0.67	0.67
NGC 6193	2444	OGLE-GD-CEP-1175*	0.70	$\varpi, \mu_{\alpha}^*, \mu_{\delta}$	1.00	0.67	0.67
NGC 6067	2370	V0340 Nor	0.20	$\varpi, \mu_{\alpha}^*, \mu_{\delta}$	1.00	0.66	0.66
BH 222	2564	OGLE-BLG-CEP-110	0.41	$\varpi, \mu_{\alpha}^*, \mu_{\delta}$	1.00	0.65	0.65
NGC 6649	2949	V0367 Set	0.73	$\varpi, \mu_{\alpha}^*, \mu_{\delta}$	1.00	0.63	0.63
Kronberger 84	3532	ASASSN-V J213533.70+533049.3	0.22	$\varpi, \mu_{\alpha}^*, \mu_{\delta}$	1.00	0.62	0.62
UBC 266	–	OGLE-GD-CEP-1676	1.08	$\varpi, \mu_{\alpha}^*, \mu_{\delta}$	0.94	0.62	0.58
FSR 1755	–	OGLE-BLG-CEP-175	1.00	$\mu_{\alpha}^*, \mu_{\delta}$	1.00	0.57	0.57
UBC 130	–	SV Vul	1.41	$\varpi, \mu_{\alpha}^*, \mu_{\delta}$	0.73	0.71	0.52
UBC 229	–	V0335 Pup	0.48	$\varpi, \mu_{\alpha}^*, \mu_{\delta}$	1.00	0.51	0.51
NGC 7790	3781	CE Cas B	0.51	$\varpi, \mu_{\alpha}^*, \mu_{\delta}$	1.00	0.50	0.50
FSR 0158	3182	GQ Vul	1.80	$\varpi, \mu_{\alpha}^*, \mu_{\delta}$	0.53	0.89	0.47
ASCC 12	427	SV Per	1.85	$\varpi, \mu_{\alpha}^*, \mu_{\delta}$	0.51	0.90	0.46
LP 1937	–	DF Cas	1.58	$\varpi, \mu_{\alpha}^*, \mu_{\delta}$	0.64	0.71	0.45
UBC 608	–	ASASSN-V J040516.13+555512.9	0.63	$\varpi, \mu_{\alpha}^*, \mu_{\delta}$	1.00	0.45	0.45
LP 1370	–	DT Gem	1.77	$\varpi, \mu_{\alpha}^*, \mu_{\delta}$	0.55	0.78	0.43
FSR 0172	3218	Dauban V16	1.49	$\varpi, \mu_{\alpha}^*, \mu_{\delta}$	0.68	0.59	0.40
NGC 6087	2382	S Nor	0.14	$\varpi, V_r, \mu_{\alpha}^*, \mu_{\delta}$	1.00	0.38	0.38
LP 2134	–	VY Per	1.53	$\varpi, \mu_{\alpha}^*, \mu_{\delta}$	0.66	0.56	0.37
LP 888	–	CE Cas B	1.91	$\varpi, \mu_{\alpha}^*, \mu_{\delta}$	0.50	0.71	0.35
LP 2134	–	UY Per	1.01	$\varpi, \mu_{\alpha}^*, \mu_{\delta}$	0.99	0.35	0.35
NGC 6631	2916	OGLE-BLG-CEP-164	1.43	$\varpi, \mu_{\alpha}^*, \mu_{\delta}$	0.71	0.46	0.33
LP 888	–	CE Cas A	1.91	$\varpi, \mu_{\alpha}^*, \mu_{\delta}$	0.50	0.66	0.33
UBC 106	–	CM Set	1.30	$\varpi, \mu_{\alpha}^*, \mu_{\delta}$	0.79	0.40	0.32
DBSB 179	2544	OGLE-BLG-CEP-173	0.66	$\varpi, \mu_{\alpha}^*, \mu_{\delta}$	1.00	0.31	0.31
IC 2395	1537	OGLE-GD-CEP-0270*	1.93	$\varpi, \mu_{\alpha}^*, \mu_{\delta}$	0.48	0.61	0.29
BH 121	1960	OGLE-GD-CEP-1688	0.91	$\varpi, \mu_{\alpha}^*, \mu_{\delta}$	1.00	0.29	0.29
UBC 291	–	OGLE-GD-CEP-1719	2.21	$\varpi, \mu_{\alpha}^*, \mu_{\delta}$	0.40	0.72	0.28
LP 888	–	CF Cas	1.98	$\varpi, \mu_{\alpha}^*, \mu_{\delta}$	0.47	0.59	0.28
NGC 7790	3781	CE Cas A	0.50	$\varpi, \mu_{\alpha}^*, \mu_{\delta}$	1.00	0.28	0.28
Ruprecht 79	1701	CS Vel	0.84	$\varpi, V_r, \mu_{\alpha}^*, \mu_{\delta}$	1.00	0.23	0.23
Loden 143	1807	OGLE-GD-CEP-0507	2.74	$\varpi, \mu_{\alpha}^*, \mu_{\delta}$	0.21	0.95	0.20
UBC 290	–	X Cru	2.04	$\varpi, \mu_{\alpha}^*, \mu_{\delta}$	0.45	0.41	0.18
Gulliver 29	–	OGLE-BLG-CEP-172	2.20	$\varpi, \mu_{\alpha}^*, \mu_{\delta}$	0.39	0.47	0.18
BH 99	1831	OGLE-GD-CEP-0507	2.99	$\varpi, \mu_{\alpha}^*, \mu_{\delta}$	0.21	0.85	0.18
UBC 406	–	CG Cas	1.72	$\varpi, \mu_{\alpha}^*, \mu_{\delta}$	0.58	0.30	0.17
Teutsch 145	2978	GDS J1842359-051557	1.66	$\varpi, \mu_{\alpha}^*, \mu_{\delta}$	0.59	0.29	0.17
LP 699	–	DK Vel	3.29	$\varpi, \mu_{\alpha}^*, \mu_{\delta}$	0.17	0.97	0.17
UBC 553	–	OGLE-GD-CEP-1196	0.90	$\varpi, \mu_{\alpha}^*, \mu_{\delta}$	1.00	0.16	0.16
UBC 80	–	ASAS J060722+0834.0	3.24	$\varpi, \mu_{\alpha}^*, \mu_{\delta}$	0.18	0.91	0.16
Schuster 1	1756	GDS J1004164-555031	2.30	$\varpi, \mu_{\alpha}^*, \mu_{\delta}$	0.36	0.44	0.16
LP 1332	–	VV Cas	2.63	$\varpi, \mu_{\alpha}^*, \mu_{\delta}$	0.29	0.55	0.16
UFMG 69	–	OGLE-BLG-CEP-057	2.98	$\varpi, \mu_{\alpha}^*, \mu_{\delta}$	0.21	0.62	0.13
Loden 153	1824	CS Car	1.71	$\varpi, \mu_{\alpha}^*, \mu_{\delta}$	0.46	0.28	0.13
UFMG 70	–	OGLE-BLG-CEP-057	1.91	$\varpi, \mu_{\alpha}^*, \mu_{\delta}$	0.49	0.27	0.13
NGC 4609	2062	WISE J124231.0-625132	1.01	$\varpi, \mu_{\alpha}^*, \mu_{\delta}$	0.99	0.13	0.13
Collinder 228	1845	OGLE-GD-CEP-1673	3.66	$\varpi, \mu_{\alpha}^*, \mu_{\delta}$	0.13	0.93	0.12
UBC 345	–	V0459 Sct	3.77	$\varpi, \mu_{\alpha}^*, \mu_{\delta}$	0.12	1.00	0.12
LP 699	–	GDS J0909005-533555	2.62	$\varpi, \mu_{\alpha}^*, \mu_{\delta}$	0.29	0.41	0.12
UBC 409	–	V0824 Cas	2.71	$\varpi, \mu_{\alpha}^*, \mu_{\delta}$	0.27	0.39	0.10
Loden 143	1807	OGLE-GD-CEP-1669	3.28	$\varpi, \mu_{\alpha}^*, \mu_{\delta}$	0.13	0.82	0.10
UBC 286	–	OGLE-GD-CEP-1707	1.36	$\varpi, \mu_{\alpha}^*, \mu_{\delta}$	0.76	0.14	0.10
LP 925	–	ASASSN-V J062542.07+082944.4	2.95	$\varpi, \mu_{\alpha}^*, \mu_{\delta}$	0.22	0.45	0.10

\* Uncertain Cepheid classification, as noted by the OGLE team.

Open clusters with identification names starting with UBC correspond to clusters found by Castro-Ginard et al. (2018, 2019, 2020). The cluster names starting with LP are discoveries of Liu & Pang (2019), whereas those starting with UFMG are from Ferreira et al. (2021). Cepheid names are taken from the International Variable Star Index (VSX, Watson, Henden, & Price 2006, 2014), or from the OGLE catalogue (Udalski et al. 2018).

missing in our catalog. Both the lists of clusters and Cepheids have been regularly updated and are much larger than the ones used for previous studies. Of course, there is always the possibility that an object is retracted, and this is actually the case for the Cepheid ASAS J155149–5621.8 (Pojmanski & Maciejewski 2004) located 0.1 deg away from the centre of the cluster NGC 5999, within its limiting radius ( $r_{\text{lim}} \sim 0.15$  deg; Ferreira et al. 2019). A potential association has been hypothesised by Chen, de Grijs, & Deng (2015), based on good agreement in proper motion, although they noted a mismatch for the computed age and distance modulus. However, the star is not considered as a classical Cepheid anymore: it is listed as a type II Cepheid by Clementini et al. (2019) and as "other" by Ripepi et al. (2019). It is considered a non-periodic variable in ASAS-SN (Jayasinghe et al. 2019b).

Another possibility is that an insignificant membership probability originates from a low prior  $P(A)$ . The projected distance between the Cepheid and the cluster centre has obviously not substantially changed, and since we opted for a looser prior, the only possibility for this to happen is that the cluster apparent size has been modified after its core radius, limiting radius, or both, were modified. This could be the case for the potential association between the Cepheid X Cyg and the cluster Ruprecht 175. This pair has been considered a bona-fide association by other authors in the past (Turner 1998a; Chen, de Grijs, & Deng 2015), but the pair's projected separation is 0.37 deg (28.6 pc, assuming membership), which, given a tabulated value of  $r_1=0.05$  deg for Ruprecht 175 (3.8 pc, K13) gives a prior probability of virtually zero. We note in addition that the difference in parallax and proper motions between the cluster and the Cepheid are about ten times higher than their respective uncertainties, which leads to a negligible association probability.

As mentioned above, updated values of the input parameters and their uncertainties with respect to those used in previous studies may result in smaller posterior probabilities, which may even become negligible and inconsistent with membership. This could have happened for the Cepheid BB Sgr, associated with the cluster Collinder 394 by many authors (Tsarevsky, Ureche, & Efremov 1966; Turner 1984; Usenko et al. 2019). It has a relatively high prior  $P(A)=0.63$ , but there is a noticeable difference in the parallax and proper motions in right ascension and declination of the cluster and the Cepheid, which are 0.20 mas, 1.83 mas yr<sup>-1</sup>, and 0.85 mas yr<sup>-1</sup>, respectively. An analogous case occurs for the combo WZ Sgr and Turner 2, where the difference in parallax and proper motions in right ascension and declination of the cluster and the Cepheid is 0.22 mas, 0.25 mas yr<sup>-1</sup>, and 0.57 mas yr<sup>-1</sup> (respectively), the latter being larger than three times the cluster's proper motion dispersion. Similarly, the Cepheid CG Cas has been considered for a long time a likely member of the cluster Berkeley 58 ( $r_{50} = 3.6$  pc, Turner et al. 2008; Chen, de Grijs, & Deng 2015), of which it is separated by 0.09 deg (5.4 pc). In spite of having  $P(A) = 0.62$ , we found a negligible membership probability for this pair due to their differences in parallax and proper motion. Interestingly, we found instead higher probabilities for CG Cas to be associated with UBC 406 (0.17) or LP 888 (0.09). In the case of CG Cas and UBC 406, the angular separation corresponds to  $1.7 \cdot r_1$  (0.17 deg; 10.6 pc, assuming membership), whereas the Cepheid is located at  $2.7 \cdot r_1$  from the centre of LP 888 (0.74 deg; 37.2 pc). We note in addition that the Cepheid V0997 Cas shows signs of an association with the cluster LP 888, albeit with a low probability of 2 per cent.

The case of RU Sct is more complicated, because the Cepheid has been associated with the cluster Trumpler 35 (Turner 1980; Chen,

de Grijs, & Deng 2015) as well as with other hosts, like Dolidze 32 (A13). In fact, A13 computed a membership probability of 0.52 with Dolidze 32 and of only 15 per cent with Trumpler 35. In our study, we obtain a prior of 0.35 and 0.04 for the association of RU Sct with Dolidze 32 and Trumpler 35, respectively, and posterior probabilities smaller than 1 per cent in both cases. These insignificant  $P(A|B)$  are mostly due to the large difference in proper motions, which exceed the uncertainties by about one order of magnitude, and due to the large radial velocity difference of 19 km s<sup>-1</sup> in the case of the pair Dolidze 32 – RU Sct, where the individual uncertainties used are 7.4 and 2 km s<sup>-1</sup>, respectively. A third possible host for RU Sct could be the cluster Dolidze 34, for which  $P(A) = 0.07$  (RU Sct lies at approximately four times the cluster's  $r_1$ ). However, in that case we also obtain an insignificant membership probability, based on a radial velocity, parallax, and proper motion comparison.

Moreover, we could end up with a very low posterior probability because uncertainties have been underestimated. This could for instance be the reason why we do not recover the Cepheid SU Cyg associated with the cluster Turner 9 (Turner et al. 1998b; Turner 2010; A13). SU Cyg is located at the centre of the cluster, which returns  $P(A)=1.0$  in our analysis. However, parallax and proper motion differences between the pair are much larger than their corresponding uncertainties (about one order of magnitude), and we obtain therefore a small association probability for Turner 9 and SU Cyg.

Hanke et al. (2020) advocate for an additional unknown systematic error on Gaia DR2 proper motions. Analyzing stars with a possible globular cluster origin, they find that, from their position in the color-magnitude diagram and their absolute proper motion deviation with respect to the globular cluster M 13's mean value (see their Figure 2), the bright stars in their sample are obvious members of M13. However, those stars would not qualify as cluster members when taking into account the relative proper motion deviation. This result is a consequence of their membership likelihoods, computed from proper motions only and based on Mahalanobis distances, becoming very small for such stars. Since those stars have  $G$  magnitudes of the order of  $G = 14 - 15$  mag, the effect might be similar for the open cluster members considered here, and even stronger for the somewhat brighter Cepheids in our sample. This could in turn artificially lower the value of our posterior probabilities.

Finally, we already mentioned in Section 3.1 that we adopted a looser prior as compared with A13 to accommodate for possible primordial or tidal features surrounding open clusters. However, it might be necessary to relax in addition the conditions related to parallaxes, proper motions, and radial velocities, in order to properly account for the dynamical state of the clusters. It could indeed be that the larger uncertainties in the pre-Gaia era were masking this effect, which could not be omitted anymore in the light of Gaia's accuracy and precision. We note in passing that inflating the uncertainties in the astrometric data by a factor of two would also increase the total number of combos with  $P(A|B) > 0.01$  by a factor of two (from 163 to 328 pairs).

### 5.3 Combos with high likelihood but low prior

In Table 1, where we list combos with probabilities higher than 0.10, the large majority of stars have a high prior. There are also a few stars with a lower prior, compensated by a high likelihood. In other words, their properties match extremely well with those of their potential host cluster, and they end up with a low probability only



due to their large projected distance to the cluster. This is for instance the case of DK Vel in LP 699, OGLE GD-CEP-0507 in Loden 143 (MWSC 1807), SV Per in ASCC 12 (MWSC 427), and V0459 Sct in UBC 345.

When inspecting stars with lower membership probabilities ( $0.01 < P(A|B) < 0.10$ , Table A1), the number of these cases increases, including for instance OGLE GD-CEP-0964 and OGLE GD-CEP-0968 in UFMG 54, RW Cam in UPK 300, and OGLE GD-CEP-1167 in UBC 545. A handful of such stars are associated with 2–4 clusters, but with high likelihoods only with 1–2 hosts, such as AQ Pup and LP 1428, and OGLE GD-CEP-1669 with Loden143 and UBC 259.

A high likelihood is obviously not a guarantee of membership, as it can in particular be driven by issues in the determination of the astrometric parameters and/or large uncertainties. Nevertheless, we highlight these cases as interesting pairs to further investigate. We note that if we do not restrict ourselves to combos with membership probabilities  $P(A|B) > 0.01$ , we find 258 additional combos with likelihood  $P(B|A) > 0.85$ . They are listed in Table A3 in the Appendix. Within this sample, 66 per cent of the stars lie within  $35 \cdot r_1$ , a value after which the distribution of projected radial distance drops drastically.

#### 5.4 Some combos of interest

In this section we select arbitrarily a small number of combos for a more detailed discussion, focusing mostly on newly discovered clusters as potential hosts (not necessarily those with the highest membership probabilities).

##### 5.4.1 Clusters potentially hosting several Cepheids

In our sample of combos with membership probabilities  $P(A|B) > 0.01$ , we find clusters that appear to be associated with several stars. We list them here below for further investigation and provide a few comments for each of them. With the current data at hand, in addition to the astrometric and kinematic constraints used in this work, we conclude that only a couple of them are robust detections.

The Cepheids AQ Pup and V620 Pup present probabilities of association with LP 1429 (Liu & Pang 2019) of 0.04 and 0.01, respectively, mostly due to their likelihoods (0.42 and 0.40). Possible associations of these Cepheids with overdensities, or putative clusters in their surroundings have been suggested in the past (Turner et al. 2012), including Ruprecht 43, Ruprecht 44, and Turner 12. We report negligible membership probabilities in these cases, even considering the relatively high prior of AQ Pup and Turner 12 (0.25).

Three Cepheids are listed with non-negligible membership probability in BH 131: OGLE GD-CEP-0785 is the closest one (at 17 pc from the cluster centre, assuming membership) and therefore also has the highest prior ( $\sim 0.43$ ), while OGLE GD-CEP-0790 and OGLE GD-CEP-0795 lie farther away, with priors of 0.12 and 0.01. Only the latter has a higher likelihood (0.82), thus the three Cepheids have an overall membership probability of only 0.01–0.02. Other clusters in the neighborhood of BH 131 are BH 132 and UBC 521. Both the priors and the likelihoods are negligible for the association of OGLE GD-CEP-0785, OGLE GD-CEP-0790, and OGLE GD-CEP-0795 with these clusters.

Collinder 228 might host four Cepheids, namely V720 Car, OGLE GD-CEP-0575, OGLE GD-CEP-1672, and OGLE GD-CEP-1673. They have priors  $> 0.10$  but relatively low likelihoods (with the exception of OGLE GD-CEP-1673) and therefore end up with membership probabilities ranging from 1 to 12 per cent.

For the Cepheids VY Per, UY Per, and SZ Cas we report a  $P(A|B)$  of 0.37, 0.35, and 0.07 with LP 2134 (Liu & Pang 2019), respectively, as a combination of their high priors and likelihoods. These relatively high membership probabilities make LP 2134 a case of interest, for which we consider further studies might be required. Other clusters within our list with which these Cepheids could be associated with because of their on-sky proximity, are Czernik 8, FSR 0591, UBC 190, ASCC 8, and SAI 17. However, for all of them the resulting  $P(A|B)$  are near zero, including the pair Czernik 8–UY Per, which has been considered a real association in previous works (e.g., Turner 1977; Chen, de Grijs, & Deng 2015). For this pair in particular, the reason for its low probability is their low  $P(B|A)$ , which is not compensated by its slightly higher, but still poor prior (0.02 per cent).

Five Cepheids are seemingly related to LP 699 (GDS J0909005-533555, DK Vel, V0530 Vel, OGLE-GD-CEP-0341, EX Vel), with combinations of priors and likelihoods leading to membership probabilities from 1 to 17 per cent, with the larger value corresponding to DK Vel. We note that four of these Cepheids, GDS J0909005-533555, DK Vel, V0530 Vel, and OGLE-GD-CEP-0341, were not included in the analysis of A13, whereas EX Vel was paired with the cluster Teutsch 48, although with a null membership probability from that work. We confirm this result. The other four Cepheids are initially crossmatched with other clusters in the field in our study. However, the membership probabilities of these pairs are not significant overall.

Finally, six Cepheids are potentially associated with LP 925, namely VW Mon, V480 Mon, V966 Mon, ASAS J062855+1107.3, OGLE GD-CEP-0040, ASASSN-V J062542.07+082944.4, but they have either a low prior or a low likelihood. Their membership probabilities range from 2 to 10 per cent, making their association with LP 925 rather unlikely.

##### 5.4.2 Gaia 5 and V0423 CMa

The Cepheid V0423 CMa lies within the half-light radius of the recently discovered cluster Gaia 5 (2 pc; Torrealba, Belokurov, & Koposov 2019). In the cluster discovery publication, the authors discard a possible association between Gaia 5 and V0423 CMa, arguing that the distance modulus difference determined in their study ( $\sim 1.7$ ) make the pair likely unrelated. We analyzed the pair based on parallaxes only, since this is the only information available for both the cluster and the Cepheid. Our method outputs a membership probability of 0.94. Translated into distances, parallax values give a distance difference of  $\sim 120$  pc only between the Cepheid and the cluster, a small value when compared with the cluster distance (6.8 kpc; Torrealba, Belokurov, & Koposov 2019).

##### 5.4.3 Kronberger 84 and ASASSN-V J213533.70+533049.3

For the first overtone Cepheid ASASSN-V J213533.70+533049.3 ( $P = 3.2$  d) we find a possible association with the cluster Kronberger 84 (MWSC 3532, K13). In this case, the Cepheid lies close to the centre of the cluster (at 0.30 pc), well within its  $r_{50}$  (0.02 deg, 1.34 pc). This results in  $P(A) = 1$ . The posterior membership probability of this pair is 0.62, as a combination of both its high prior and likelihood. As a list of members of this cluster is provided by CG20, we display in Figure A1 the astrometry and color-magnitude diagram of this pair to illustrate its compatibility.

#### 5.4.4 UBC 130 and SV Vul

SV Vul falls in a region of the sky with numerous clusters and star-forming regions, including Vul OB1 with which the Cepheid has been associated for a long time (Turner 1984). We find a high probability of association ( $\sim 0.52$ ) between SV Vul and the open cluster UBC 130 (Castro-Ginard et al. 2020). The distance of SV Vul to the centre of UBC 130 is 6 pc (0.15 deg) assuming membership, about 50 per cent larger than the cluster's  $r_{50}$ . It turns out that UBC 130 is another designation for the cluster Alicante 13, for which the membership of SV Vul has been recently demonstrated by Nequeruela, Dorda, & Marco (2020). The astrometric parameters of SV Vul as compared with those of the members of UBC 130 (CG20) are depicted in Figure A1.

#### 5.4.5 UBC 229 and V0335 Pup

The angular separation between the Cepheid and the cluster's centre (0.04 deg) corresponds to 1.8 pc assuming membership, which locates V0335 Pup within the  $r_{50}$  of UBC 229 (3.6 pc) and secures a prior of  $P(A)=1$ . The constraints analysed in this case are the pair's parallaxes and proper motions (Figure A1). They lead to an association probability of 0.51. Moreover, the position of the Cepheid in the CMD of UBC 229 and its distance are both compatible with membership.

#### 5.4.6 LP 1937 and DF Cas

DF Cas is located at 0.24 deg of the centre of the newly discovered cluster candidate LP 1937 (Liu & Pang 2019), within the cluster's  $r_2$  (0.486 deg; 25.2 pc). The value of  $P(A)$  for this pair is 0.64, and the small  $\varpi$ ,  $\mu_{\alpha}^*$ , and  $\mu_{\delta}$  differences between the Cepheid and the cluster yield a likelihood  $P(B|A)$  of 0.71, hence a posterior membership probability of 0.45. We note the presence of other clusters in the neighborhood, such as NGC 1027, for which we get a membership probability  $< 0.01$  ( $P(A)=0.77$ ,  $P(B|A) \sim 0$ ), in agreement with the results of A13.

#### 5.4.7 UBC 106 and CM Sct

We find a prior of 0.79 and a likelihood of 0.40 for CM Sct, hence a membership probability to UBC 106 of 0.32, based on parallax and proper motion. CM Sct is located outside of the cluster's  $r_{50}$  ( $\sim 4.9$  pc or 0.12 deg), with a physical distance of 6.6 pc assuming the cluster and the Cepheid equidistant. The position of the Cepheid in the cluster's colour-magnitude diagram is compatible with membership (Figure A1). We highlight this combo as A13 report a high likelihood for the combos CM Sct/Dolidze 32 and CM Sct/Dolidze 33, but with small membership probabilities of  $< 1$  and 1.6 per cent, respectively. Their probability is slightly higher with Teutsch 145 (2.8 per cent) thanks to a higher prior (0.21), but with a reduced likelihood of 0.13. We checked that the aforementioned clusters are distinct from UBC 106.

Our results indicate another Cepheid potentially associated with UBC 106, Z Sct, which is located  $\sim 700$  pc away in heliocentric distance from CM Sct (and half a degree away on the sky) and has similar likelihood but a much lower prior than CM Sct. With an angular separation between Z Sct and the centre of UBC 106 (0.48 deg, which corresponds to 19.7 pc), the membership probability drops below 0.01. We note that the period of Z Sct is significantly larger than that of CM Sct, making it significantly younger. Our determination of the age of UBC 106 shows a quite large uncertainty,

but overall matches  $\log(t) = 8.2$  provided by CG20. It then also supports a higher membership probability for CM Sct than for Z Sct, whatever the PA relation we consider. We note in passing that A13 mention Z Sct in eight potential combos, all of them with negligible membership probability although with a likelihood  $P(B|A) = 1$  for three of them (Dolidze 32, Dolidze 33, Andrews-Lindsay 5).

#### 5.4.8 UBC 290 and X Cru

The combo composed of the cluster UBC 290 (Castro-Ginard et al. 2020) and the fundamental-mode pulsator X Cru ( $P = 6.22$  d) is another case of a relatively high  $P(A|B)$  association, as the Cepheid lies at 8.6 pc from the center of the cluster of size  $r_{50} = 0.15$  deg (4.24 pc), which, together with a high likelihood, yields a posterior probability of 0.18 (Figure A1). We note that neither the cluster nor the Cepheid are included in the study of A13.

## 6 AGE DETERMINATION OF OPEN CLUSTERS

In this section, we derive ages for a subsample of clusters believed to host Cepheids in the literature, or where the Cepheid has a high membership probability according to our study (see Section 5, and Table 1). We compare these estimates with age determinations from the literature, and check their consistency with theoretical Cepheid pulsation and evolution models.

### 6.1 Methodology

Age-dating resolved star clusters via isochrone fitting is a task for which several techniques have been used along the years, from pure visual inspection to recently developed algorithms (see e.g., von Hippel et al. 2006; Monteiro, Dias, & Caetano 2010; Dias et al. 2012; Liu & Pang 2019; Sim et al. 2019; CG20). In most cases, the codes used for these calculations are not made publicly available. However, in spite of the application of new methodologies, determining the age of young clusters remains as a challenging goal because in addition to stellar contamination, binarity, and age spreads, the MSTO of these clusters is commonly not clearly defined.

We adopted two approaches: a  $\chi^2$ -based isochrone selection developed on our own, and the AURIGA neural network (henceforth ANN; Kounkel, Covey, & Stassun 2020), which predicts the age, extinction, and distance of clusters from the photometry and astrometry of the cluster members. We did not use the software BASE 9 (von Hippel et al. 2006) as in Bossini et al. (2019) since these authors mention that its use together with only Gaia magnitudes does not allow one to lift the degeneracy between the distance modulus and the extinction.

For our own method, we used the PAdova and TRieste Stellar Evolution Code (PARSEC; Bressan et al. 2012) stellar evolution models. The models were computed for the Gaia DR2 passbands (Evans et al. 2018), and in the 2MASS photometric system. From the available models, we selected evolutionary tracks with initial chemical compositions ranging from  $Z = 0.006$  to  $Z = 0.029$  and a grid size of 0.001 dex. Approximately 90 per cent of the clusters in the catalogue of Carrera et al. (2019) younger than 800 Myr (with ages from CG20) lie in this range of  $Z$ . The ages selected vary from  $\log(t) = 6.6$  ( $\sim 5$  Myr), with  $t$  in units of years, to  $\log(t) = 8.9$  ( $\sim 800$  Myr) with a minimum resolution of 0.01 dex, including extreme values of  $\log(t)$  for a proper uncertainty determination. Since rotationally-induced instabilities strongly affect the evolution of stars, as studied

specifically in the case of Cepheids by [Anderson et al. \(2016\)](#), we also adopted models that take stellar rotation into account, namely the MESA Isochrones and Stellar Tracks (MIST) set of evolutionary tracks, which are based on the publicly available stellar evolution tool Modules for Experiments in Stellar Astrophysics (MESA; [Paxton et al. 2011, 2013; Dotter 2016; Choi et al. 2016](#)). We chose evolutionary tracks with a range of initial iron abundances [Fe/H] from  $-0.5$  to  $0.5$  with a grid size of  $0.25$ , and logarithmic ages between  $6.6$  and  $8.9$ , with a step size of  $0.05$  dex.

The selection of the best model isochrone for a given cluster is based on a  $\chi^2$  minimization criterion when comparing it with the cluster colour-magnitude diagram<sup>4</sup>. We repeated the process twice, first using Gaia photometry only and then using 2MASS photometry only. In the latter case, the near-infrared  $J$ ,  $H$ , and  $K$  magnitudes of the cluster members are taken from [Roesser, Demleitner, & Schilbach \(2010\)](#).

In order to perform the isochrone fitting, we limited ourselves to cluster members as established in previous studies, and we discarded clusters for which the main sequence was not clearly defined. In the case of the clusters in CG18b, who provide a membership probability, we included all stars with membership probabilities larger than 30 per cent and within  $2.5 \cdot r_1$  from the cluster centre. For the clusters from [Castro-Ginard et al. \(2020\)](#), we simply used the list of members provided by the authors. Additionally, a number of stars was further excluded during the fitting process via sigma-clipping. As initial conditions for the fitting routine, we adopted the values provided in the literature. From this original value, we explored an age window of  $\pm 0.5$  in logarithmic scale, using  $0.05$  as a grid size and a metallicity window of  $\pm 0.03$  dex in  $Z$ , with a grid size of  $0.01$  dex. For the reddening, we allowed for an excursion of  $\pm 0.6$  mag from the initial value, in steps of  $0.15$  mag. The extinction values were computed assuming  $R_V = 3.1$  ([Schultz & Wiemer 1975; Cardelli, Clayton, & Mathis 1989](#)), adopting the ratios  $A_G/A_V = 0.85926$ ,  $A_{GBP}/A_V = 1.06794$ ,  $A_{GRP}/A_V = 0.65199$ ,  $A_J/A_V = 0.29434$ ,  $A_{HG}/A_V = 0.18128$ , and  $A_K/A_V = 0.11838$ <sup>5</sup>, and without considering differential reddening. Finally, we allow distances to vary in a range of  $\pm 500$  pc from the initial value, in steps of  $50$  pc.

To account for the magnitude errors on the stars'  $G$ ,  $G_{BP}$ , and  $G_{RP}$  magnitudes, we assumed:

$$\sigma_{\text{mag}}^2 = (1.09 \frac{\sigma_{\text{Flux}}}{\text{Flux}})^2 + \sigma_{\text{zp}}^2 \quad (9)$$

where  $\sigma_{\text{mag}}$  is the magnitude error of a star in a given Gaia bandpass,  $\text{Flux}$  is the mean flux of the star in that filter, and  $\sigma_{\text{Flux}}$  its uncertainty. We used this formula since no errors are provided in the Gaia catalogues because of the asymmetric error distribution of the sources in magnitude space, as stated in the table description of the Gaia DR2<sup>6</sup>. We adopted  $\sigma_{\text{zp}} = 0$  as we possess no knowledge of the behaviour of this zero-point, and its effects should be negligible for the purpose of our study.

The uncertainties on the age determination were estimated by inspecting the distribution of the minimum  $\chi^2$  as a function of age in the range explored for a given cluster. We computed the significance of the global minimum by looking for the local maxima around it, allowing asymmetric errors if necessary.

In a few cases, when the fit appeared inconsistent with the cluster members in a visual inspection, we applied small adjustments,

setting the age to a local rather than a global minimum or correcting for small distance/reddening imprecisions when the best value would fall in between two consecutive grid points. We did so for seven clusters analyzed with Gaia photometry and PARSEC isochrones, five clusters with Gaia photometry and MIST isochrones, two clusters with 2MASS photometry and PARSEC isochrones, and four clusters with 2MASS photometry and MIST isochrones. The median shift in age is  $0.20$  in logarithmic scale, with a maximum of  $0.60$  for the cluster Ruprecht 100 in a Gaia+PARSEC configuration. The case of Ruprecht 100 in the 2MASS+PARSEC configuration remained nevertheless an unsatisfactory fit and was fitted using a visual inspection only, as displayed in Figure 4.

Alternatively, we employed the ANN<sup>7</sup> to derive the cluster properties. The ANN is a neural network trained on a mix of artificial stellar populations and real clusters. We provided as input for each cluster photometry in the Gaia and near-infrared bands ( $G$ ,  $BP$ ,  $RP$ ,  $J$ ,  $H$ ,  $K$ ), and the Gaia DR2 parallaxes. [Kounkel, Covey, & Stassun \(2020\)](#) indicate that the ANN underestimates the age for clusters older than  $\sim 120$  Myr and overestimates it for clusters younger than  $\sim 120$  Myr, in both case by  $\sim 0.1$  dex. They remark that this threshold roughly corresponds to the age at which all low-mass pre-main sequence stars would have reached the main sequence, and very few high-mass stars would have evolved off the main sequence towards the RGB. Unfortunately, this is also the expected age range for clusters hosting Cepheids. In general, neural networks do not provide uncertainties in the predicted parameters. However, it is possible to treat the scatter between the solutions from independent realizations as a measure of these errors. Thus, for each cluster we ran 100 ANN iterations to estimate the parameter uncertainties. For more details about the ANN design, we refer the reader to [Kounkel, Covey, & Stassun \(2020\)](#).

## 6.2 Results and comparison with previous studies

It is no surprise that our analysis of clusters hosting Cepheids provides only young ages, ranging from  $\log(t)=7.4$  (25 Myr) to  $\log(t)=8.8$  (630 Myr), depending on the cluster, the method and the data considered. For reasons that will become clear later in this Section, we discuss here and list in Table 2 only 11 clusters (12 Cepheids) whose ages are considered relatively reliable (considering the accuracy and precision of the estimations) and with which we could potentially constrain the Cepheid period-age relation (see Section 6.4). Figure 5 displays the results for two representative clusters. The first one, NGC 6067, is a relatively evolved system with a well-defined main sequence, two Cepheids, and already a number of stars populating the RGB. With such favorable circumstances, all analyses lead to a similar age between  $\log(t)=7.9$  (80 Myr) and  $\log(t)=8.3$  (200 Myr). The second one, Collinder 394, is in contrast less massive, it contains only one Cepheid and no other evolved member has been reported in Gaia DR2 so far. Fortunately, it possesses a narrow main sequence and a quite well defined MSTO, allowing for a similar dispersion ( $\sim 0.4$  dex) around an age of  $\log(t)\approx 8.05$  (110 Myr). The resulting isochrones and cluster colour-magnitude diagrams of our whole sample are shown in the Appendix (Figure A2). It is clear that our "good" sample is biased toward higher ages since we report  $\log(t) < 7.8$  for only two clusters.

In the rest of this subsection we compare the age estimates from our first approach with previous studies, namely the compilations of D02 and K13, the analysis of [Bossini et al. \(2019\)](#) who derived

<sup>4</sup> The Cepheids were excluded from the computation of the  $\chi^2$  values.

<sup>5</sup> [http://stev.oapd.inaf.it/cgi-bin/cmd\\_3.3](http://stev.oapd.inaf.it/cgi-bin/cmd_3.3)

<sup>6</sup> <https://dc.zah.uni-heidelberg.de/tableinfo/gaia.dr2light>

<sup>7</sup> <https://github.com/mkounkel/Auriga>



**Table 2.** Ages for a reliable subsample of clusters. We show the logarithmic cluster ages obtained with two sets of isochrones (PARSEC or MIST) using either Gaia DR2 or 2MASS photometry, and those obtained with ANN using Gaia DR2 and 2MASS simultaneously.

Open cluster	Cepheid	Period <sup>1</sup> [days]	Pulsation Mode <sup>1</sup>	log( <i>t</i> )						Lit. log( <i>t</i> ) Bossini et al. (2019)
				GDR2 PARSEC	GDR2 MIST	2MASS PARSEC	2MASS MIST	ANN	CG20 <sup>2</sup>	
Collinder 394	BB Sgr	6.64	F	7.95 <sup>+0.20</sup> <sub>-0.40</sub>	8.05 <sup>+0.20</sup> <sub>-0.25</sub>	7.80 <sup>+0.30</sup> <sub>-0.30</sub>	8.20 <sup>+0.15</sup> <sub>-0.15</sub>	8.01 ± 0.09	7.96	7.97 <sup>+0.06</sup> <sub>-0.02</sub>
NGC 5662	V Cen	5.49	F	7.95 <sup>+0.20</sup> <sub>-0.15</sub>	7.95 <sup>+0.15</sup> <sub>-0.15</sub>	7.85 <sup>+0.25</sup> <sub>-0.25</sub>	8.45 <sup>+0.30</sup> <sub>-0.20</sub>	8.22 ± 0.12	8.30	–
NGC 6067	QZ Nor	3.79	1O	7.90 <sup>+0.50</sup> <sub>-0.30</sub>	8.00 <sup>+0.35</sup> <sub>-0.40</sub>	8.20 <sup>+0.30</sup> <sub>-0.35</sub>	8.10 <sup>+0.45</sup> <sub>-0.20</sub>	8.30 ± 0.14	8.10	–
NGC 6067	V0340 Nor	11.29	F	7.90 <sup>+0.50</sup> <sub>-0.70</sub>	8.00 <sup>+0.35</sup> <sub>-0.40</sub>	8.20 <sup>+0.30</sup> <sub>-0.35</sub>	8.10 <sup>+0.45</sup> <sub>-0.20</sub>	8.30 ± 0.14	8.10	–
NGC 6087	S Nor	9.75	F	7.75 <sup>+0.70</sup> <sub>-0.70</sub>	7.90 <sup>+0.20</sup> <sub>-0.20</sub>	7.90 <sup>+0.35</sup> <sub>-0.35</sub>	8.05 <sup>+0.55</sup> <sub>-0.20</sub>	7.92 ± 0.10	8.00	8.05 <sup>+0.02</sup> <sub>-0.03</sub>
NGC 6649	V367 Sct	6.29 (4.38)	F1O	7.45 <sup>+0.20</sup> <sub>-0.20</sub>	7.40 <sup>+0.60</sup> <sub>-0.60</sub>	7.75 <sup>+0.20</sup> <sub>-0.20</sub>	7.70 <sup>+0.35</sup> <sub>-0.35</sub>	7.18 ± 0.39*	7.85	–
Ruprecht 79	CS Vel	5.90	F	7.80 <sup>+0.25</sup> <sub>-0.20</sub>	7.80 <sup>+0.35</sup> <sub>-0.35</sub>	7.90 <sup>+0.60</sup> <sub>-0.60</sub>	7.60 <sup>+0.55</sup> <sub>-0.40</sub>	7.77 ± 0.24	7.79	–
Ruprecht 100	TY Cru	5.00	F	8.40 <sup>+0.10</sup> <sub>-0.60</sub>	8.00 <sup>+0.55</sup> <sub>-0.10</sub>	† 8.20 <sup>+0.35</sup> <sub>-0.35</sub>	8.25 <sup>+0.25</sup> <sub>-0.25</sub>	8.55 ± 0.23	8.31	–
UBC 106	CM Sct	3.92	F	8.20 <sup>+0.30</sup> <sub>-0.15</sub>	8.15 <sup>+0.25</sup> <sub>-0.15</sub>	8.00 <sup>+0.35</sup> <sub>-0.35</sub>	7.85 <sup>+0.25</sup> <sub>-0.25</sub>	7.96 ± 0.43	8.20	–
UBC 130	SV Vul	44.88	F	7.45 <sup>+0.15</sup> <sub>-0.40</sub>	7.20 <sup>+0.15</sup> <sub>-0.15</sub>	7.40 <sup>+0.30</sup> <sub>-0.30</sub>	7.20 <sup>+0.40</sup> <sub>-0.30</sub>	7.53 ± 0.32*	7.44	–
UBC 156	V1077 Cyg	4.64	F	8.80 <sup>+0.65</sup> <sub>-0.65</sub>	8.45 <sup>+0.30</sup> <sub>-0.50</sub>	8.60 <sup>+0.15</sup> <sub>-0.55</sub>	8.80 <sup>+0.35</sup> <sub>-0.35</sub>	8.19 ± 0.18	8.40	–
UBC 290	X Cru	6.22	F	8.05 <sup>+0.20</sup> <sub>-0.35</sub>	7.90 <sup>+0.35</sup> <sub>-0.35</sub>	8.00 <sup>+0.35</sup> <sub>-0.35</sub>	7.80 <sup>+0.10</sup> <sub>-0.10</sub>	7.83 ± 0.11	8.28	–

<sup>1</sup> From Ripepi et al. (2019), except for R Cru, V367 Sct (VSX, Watson, Henden, & Price 2014) and for OGLE-GD-CEP-1012 (OGLE, Udalski et al. 2018).

In the pulsation mode column, F stands for fundamental mode, 1O for first overtone, and F1O for double-mode. For the double mode Cepheid V367 Sct the first overtone period is shown in parentheses.

<sup>2</sup> The uncertainties associated with the log(*t*) determinations of CG20 range from 0.1 to 0.25 dex.

† Unsatisfactory  $\chi^2$  fitting procedure. Age determined by visual inspection.

\* Clusters for which high values of the extinction  $A_V$  ( $>1.6$ , CG20;  $>1.9$ , ANN) affected the ANN parameter determination.

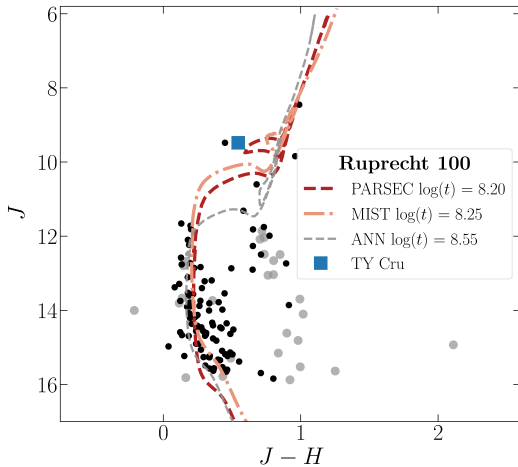


**Figure 4.** Color-magnitude diagram of the cluster Ruprecht 100, with PARSEC (red) and MIST (orange) isochrones fitted (as an exception) by visual inspection. Cluster members are taken from CG18b and shown as grey filled circles, while the cleaned sample of stars used during the isochrone fitting procedure is shown as black dots. For this cluster, automatic fits based on a  $\chi^2$  minimization did not converge to an acceptable solution, even when allowing for a manual shift of the age. A PARSEC isochrone computed with the parameters derived by the ANN analysis and assuming solar metallicity is also plotted in grey.

ages for 269 low reddening (not very young) Galactic open clusters using Gaia DR2 data (two clusters in common with our work), and the recent work of CG20 who used an artificial neural network to determine the ages of 1,867 clusters from Gaia DR2 photometry. The outcome of the comparison is shown in Figure 6, from which

we draw the following conclusions (which we emphasize are drawn from low number statistics):

- we find an overall agreement between all the literature ages we compared our results with (within 0.8 dex);
- the agreement of our ages with D02 is better than that our agreement with K13, most likely due to the cluster membership selection. The median absolute differences are 0.16 and 0.33 in logarithmic scale, respectively, for the seven clusters in common with both works;
- we reach an overall good agreement with the Bossini et al. (2019) (two clusters in common) and CG20 age estimates (11 clusters in common, median absolute difference of 0.15 dex). However, for clusters younger than log(*t*)~8.0 (100 Myr), our ages tend to be lower than those of CG20, and higher for log(*t*) > 8.2 (~160 Myr);
- there are no other clear trends of  $\Delta \log(t)$  as a function of log(*t*);
- the choice of a specific isochrone set (PARSEC or MIST) seems to have marginal influence.

We believe that the age difference between earlier studies (as compiled by D02 and K13) and the more recent ones resides mainly in the capability to select the cluster membership based on Gaia DR2 parallaxes and proper motions. However, the assumed reddening and distance for each cluster (in both earlier and recent studies) likely play an important role as well. Finally, we consider important to keep in mind the typical values of  $\Delta \log(t)$  when analysing the cluster ages from different works (and their spread), in particular for interpreting the results shown in Section 6.4.

### 6.3 A critical view on cluster Cepheids to calibrate period-age relations

To illustrate the difficulty of deriving accurate ages for young open clusters, we study the theoretical behaviour of the stellar occupation of the members of a given cluster in the Gaia colour-magnitude dia-

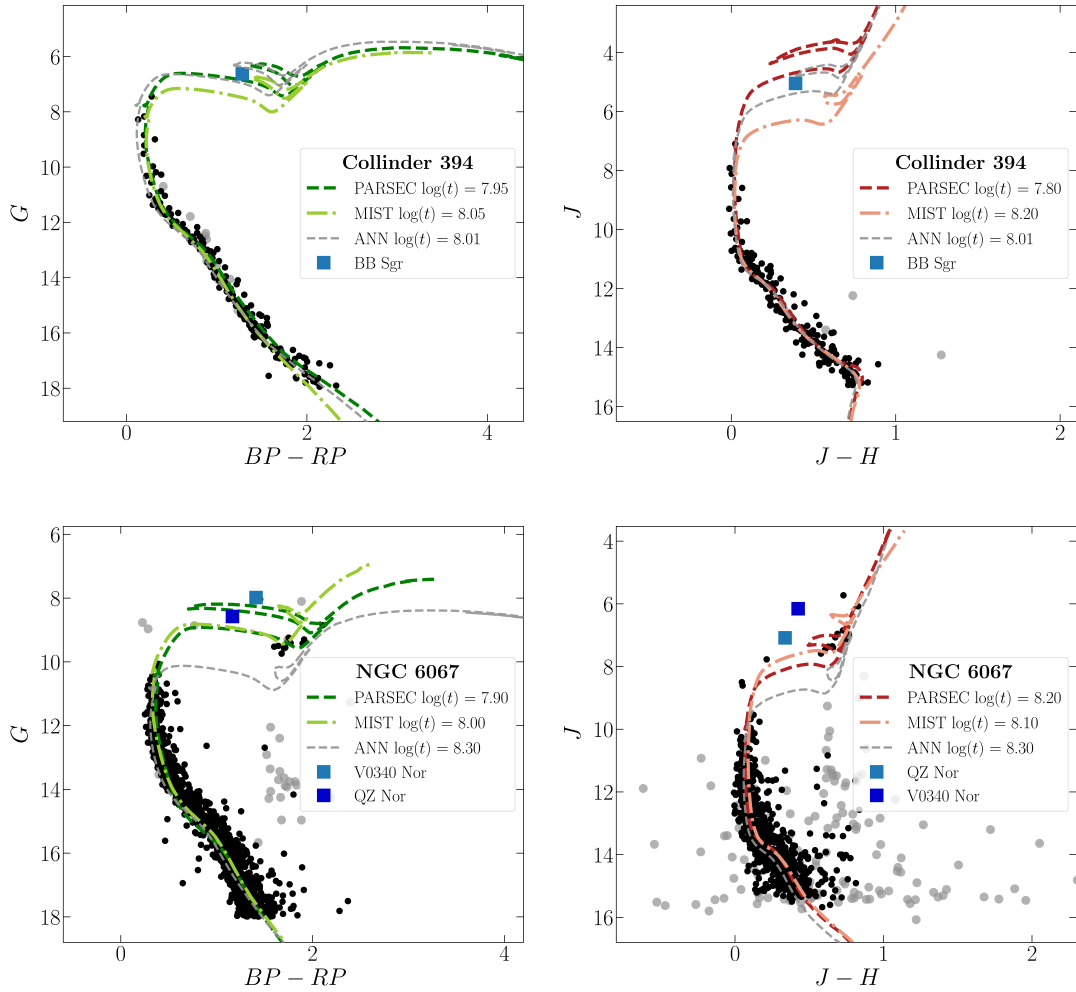


**Figure 5.** Colour-magnitude diagrams of two clusters: Collinder 394 (top panels) and NGC 6067 (bottom panels) representative of clusters hosting Cepheids. The left panels show colour-magnitude diagrams in the Gaia passbands while the right panels display them in the 2MASS passbands. Presumed cluster members from the input catalogues are shown as grey filled circles while those selected by sigma-clipping during the isochrone fitting procedure are shown as black dots. The best-fit isochrones are shown with a colour-code related to the photometric system and the stellar evolution model used in the analysis. We also show in grey a PARSEC isochrone computed with the parameters derived by the ANN analysis and assuming solar metallicity.

gram, using simple models based on stellar population synthesis. We used PARSEC isochrones to generate ten simulated clusters of solar metallicity at two specific ages (five random realizations per age). The ages selected for these models are 7.4 to 8.2 in logarithmic scale (approximately 25 and 160 Myr, respectively), for a massive Galactic open cluster ( $1,000 M_{\odot}$ ; based on the cluster mass functions shown by, e.g., Lada & Lada 2003, Zinnecker et al. 2009, and Röser et al. 2010). To compute the stellar occupation along the isochrones we adopted a Chabrier (2001) initial mass function (IMF), together with a Salpeter (1955) IMF for stars with masses larger than a solar mass. To transform the modeled absolute magnitudes to apparent magnitudes, we assumed a distance of 1 kpc, and  $E(B - V) = 0.175$ , which are representative values for a Galactic cluster such as NGC 6087. We included photometric uncertainties based on the typical magnitude errors for the NGC 6087 members in the Gaia passbands, re-drawing the magnitudes assuming Gaussian distributions. In addition, we adopted a binary fraction of 0.6 to roughly reproduce the characteristic widening produced in the evolutionary tracks by

the presence of binary companions. Finally, we added field contamination (foreground/background) based on the Besançon models<sup>8</sup> (Robin et al. 2003; Czekaj et al. 2014; Robin et al. 2014) of Galactic stellar populations for the Gaia magnitudes, including only a random selection of stars with distances between 0.8 and 1.2 kpc as possible contaminants. The results of this exercise are depicted in Figure 7.

Isochrones of different ages, in the ideal scenario in which the true distance, reddening, and metallicity of the cluster are known, are fitted to the populations plotted in the different panels of Figure 7. The scatter in the fitted logarithmic ages with respect to the isochrone ages from which the populations are drawn shows the sensitivity to different effects (e.g., photometric errors and contamination) of the age determination of a stellar cluster via isochrone fitting, and one expects it to only increase if small variations in the isochrone distances and reddenings were allowed.

A factor that is not being considered here is related to the fraction

<sup>8</sup> [https://model.obs-besancon.fr/modele\\_home.php](https://model.obs-besancon.fr/modele_home.php)

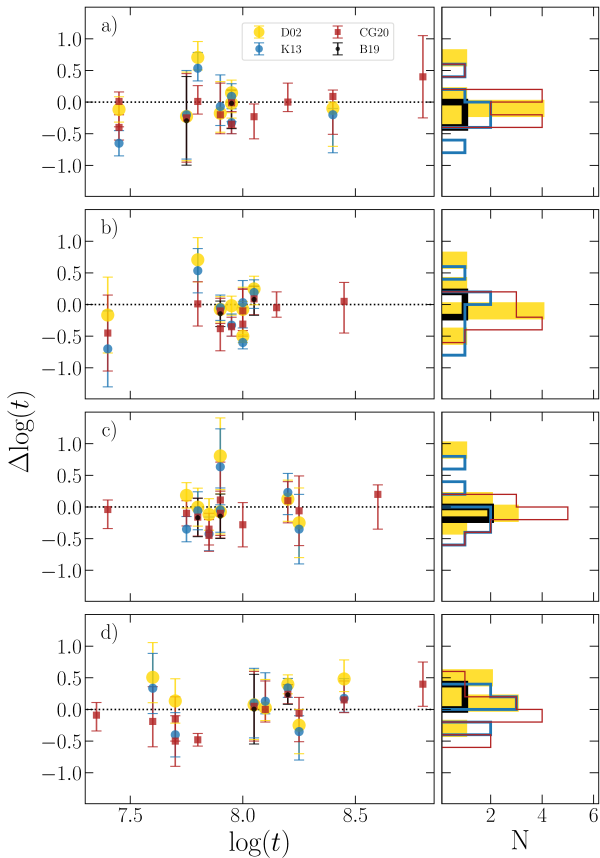


**Figure 6.** *Left panels:* Difference in logarithmic ages,  $\Delta \log(t)$ , between the values obtained in this work and those published in previous studies, for the sub-sample of clusters shown in Table 2. *Right panels:* Dispersion of the residuals in  $\Delta \log(t)$  using a bin size of 0.25 in age logarithmic scale. The sources of literature ages are D02 (yellow), K13 (blue), Bossini et al. (2019) (B19, black), and CG20 (red). The panels from top to bottom display: *a*): our ages from PARSEC isochrones, using Gaia photometry, *b*): our ages from MIST isochrones, using Gaia photometry, *c*): our ages from PARSEC isochrones, using 2MASS photometry, *d*): our ages from MIST isochrones, using 2MASS photometry. The error bars take into account the age uncertainties from this work and from the literature, when available.

of observed stars that are recovered from the theoretical stellar populations, due to the survey photometric completeness, or to possible biases in the cluster census made by the studies that selected cluster members. In the example populations depicted in Figure 7 it can be seen that, for a 25 Myr old cluster ( $\log(t) = 7.4$ ) with  $1,000 M_{\odot}$ , missing only a couple of bright members near the MSTO of the cluster might easily result in an age determination offset of 75 Myr (0.6 in logarithmic scale). Therefore, for the younger clusters in our sample, large age uncertainties are expected to be found, making them inadequate as observable checks of the PA relation of Cepheids.

In this regard, since the initial mass functions are sampled stochastically, fewer stars are formed overall in less massive clusters, and as a consequence, the probability of forming intermediate and high-mass stars decreases, especially when the star formation rate of a cluster is rather low (see, e.g., Weidner & Kroupa 2006; Eldridge 2012). In fact, the stochastic sampling that affects the observed mock cluster colour-magnitude diagrams coupled with the relatively young age of the clusters, in addition to the natural limitations of the Gaia photometry (saturation, for instance, and crowding for distant clus-

ters; Boubert & Everall 2020), translates into not well defined stellar main-sequence turn-offs and an evident dearth of cluster members at the turn-offs and post-main-sequence evolutionary stages. For more details regarding the effects of stochasticity in cluster populations we refer the reader to more dedicated works, such as those carried out by Fouesneau & Lançon (2010) and Popescu & Hanson (2010).

As a final remark, we would like to highlight that in order to overcome the limitation described above, extremely high levels of both purity and completeness in the open cluster member catalogues are mandatory for an age determination at the accuracy required (a few tens of Myr) to constrain Cepheid PA relations. In particular, no turn-off or further evolved members should be missing or falsely included. The use of reliable spectral types, in addition to high-precision reddening estimates should become beneficial to better constrain the cluster ages. If these requirements are not met, only such clusters with well-defined MSTO can in practice be used with confidence, which biases the cluster Cepheid sample selection towards older and more massive hosts. Similar conclusions were reached by Senchyna et al. (2015) in their study of the PA relation of Cepheids in M31, in which they attribute the broad constraints in their PA fits to the difficulty of assigning an age to low-mass clusters at large distances.

This is a reason why, from all the high probability combos obtained in Section 5, we retain only 11 cluster-Cepheid pairs in an attempt to characterize Cepheids' PA relations in the next section.

#### 6.4 The Cepheid Period-Age Relation

Bono et al. (2005) provided the first theoretical PA relations for Cepheids with Magellanic or solar-like chemical compositions. More recently, models including rotation have been developed (Anderson et al. 2014, 2016) predicting that, as rotation increases the main-sequence lifetime of the stars, higher Cepheid ages are expected in comparison with ages determined using non-rotating models (by  $\Delta \log(t) \sim 0.2$  to  $0.3$ ). Taking advantage of updated evolutionary (Hidalgo et al. 2018) and pulsation (De Somma et al. 2020a) models, De Somma et al. (2020b) derived new period-age relations and period-age-colour relations in the Gaia passbands.

It is natural to overlay the age of a cluster Cepheid as provided by the determination of the age of the hosting cluster (following the traditional assumption that they are coeval) on the prediction of the Cepheids' age as given by a theoretical PA relation. As described above, we take into account only those (11) clusters for which we consider the ages relatively well constrained. Considering this small number together with their bias towards larger ages, we do not consider fitting an empirical PA relation. For the same reason, we only consider fundamental mode Cepheids, since only a single first overtone Cepheid falls in this restricted sample.

The comparison with the theoretical PA relations of Bono et al. (2005) (no stellar rotation), Anderson et al. (2016) ( $\Omega_{ZAMS}/\Omega_{crit} = 0.5$ ), and De Somma et al. (2020b) (no rotation) is displayed in Figure 8. Assuming a PA relation of the shape  $\log(t) = \alpha + \beta \cdot \log(P)$ , where the value of the age  $t$  is represented in years, the former study reports  $\alpha = 8.41 \pm 0.10$  and  $\beta = -0.78 \pm 0.01$  for fundamental-mode Cepheids and for  $Z = 0.01$  (Table 4 in Bono et al. 2005). In the case of Anderson et al. (2016) we used the average PA relation slope and intercept for a Cepheid with  $Z = 0.014$  in their second and third crossing of the instability strip (Table 4 in Anderson et al. 2016), where  $\alpha = 8.48 \pm 0.09$  and  $\beta = -0.59 \pm 0.09$  for fundamental mode Cepheids. The uncertainty assumed represents the standard deviation of these values with respect to the averages. Finally, for the models of De Somma et al. (2020b) we adopt the results obtained in the case of a canonical mass-luminosity relation, when neglecting rotation,



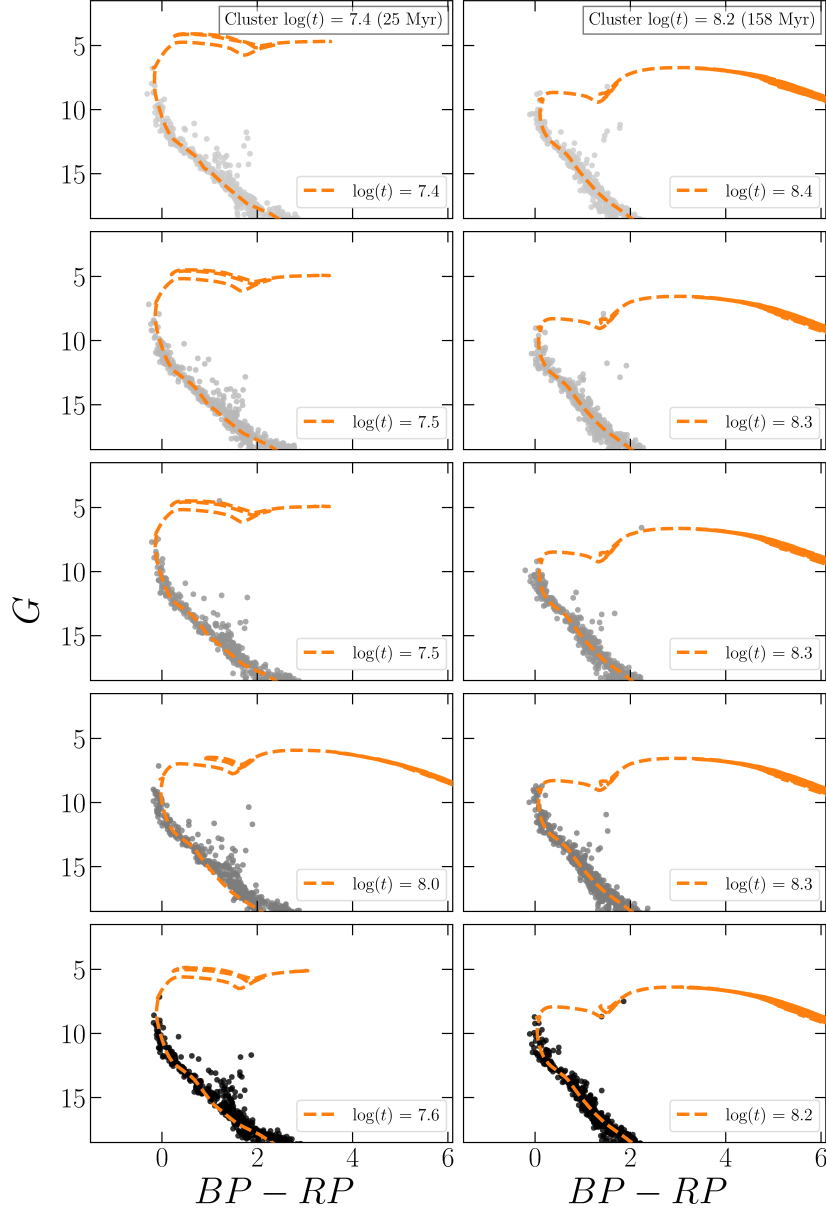


**Figure 7.** Simulated colour-magnitude diagrams for a cluster of  $\log(t) = 7.4$  (left panels) and  $\log(t) = 8.2$  (right panels), and a total initial mass of  $1,000 M_{\odot}$ . Each panel shows a different population randomly generated using a [Chabrier \(2001\)](#) + [Salpeter \(1955\)](#) IMF. Observational effects, such as photometric errors, the presence of a binary sequence, and field contamination are included in each diagram. PARSEC isochrones are fitted to the observed CMDs and displayed with orange dashed lines. The isochrones were fitted assuming the exact same distance, extinction, and metal content as those of the theoretical population, but allowing for shifts in age.

mass-loss, and overshooting, with a mixing length parameter equal to 1.5, and  $Z = 0.020$  (Table 2 in [De Somma et al. 2020b](#)). In this case  $\alpha = 8.39 \pm 0.01$  and  $\beta = -0.70 \pm 0.01$  for fundamental-mode Cepheids.

From the plots shown in [Figure 8](#), we do not observe well-defined relations between the Cepheid periods and the cluster ages, regardless of the choice of photometric system, isochrone models (with and without stellar rotation), or source of the cluster ages (from the use of the ANN, or from CG20). The large scatter of the cluster ages as compared to the theoretical predictions for the Cepheids' ages reveals the lack of accuracy and precision of our age determinations for this purpose, and makes it impossible to discriminate between

the various theoretical Cepheid PA relations. Although not a factor here, we stress that a proper comparison between theoretical and empirical ages should be carried out with models making the same assumptions on overshooting, rotation, etc.

## 7 DISCUSSION AND CONCLUDING REMARKS

Considering that the number of known open clusters and classical Cepheids has increased considerably in recent years, and taking advantage of the unprecedented quality of the data provided by the Gaia mission (DR2 and eDR3), we revisited the membership of classical

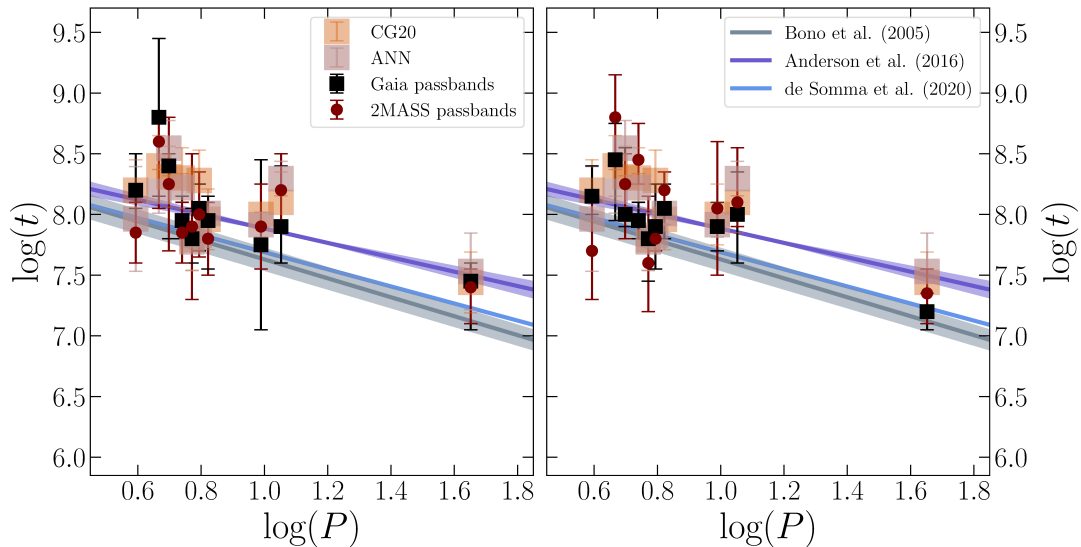


**Figure 8.** Comparison between the logarithm of the Cepheid periods in days (Udalski et al. 2018; Ripepi et al. 2019) and the cluster logarithmic ages (in years), obtained with different isochrone sets: PARSEC (left panel) and MIST (right panel) for the combos shown in Table 2. We do not include in the plot the unique first overtone Cepheid recovered as high probability cluster member. Black symbols represent the cluster ages obtained using Gaia DR2 photometry and red stars those obtained using the 2MASS passbands. For comparison, we overplot these values to the theoretical PA relation for fundamental-mode Cepheids derived by Bono et al. (2005), in gray, Anderson et al. (2016), in blue, and De Somma et al. (2020b) in light blue, for  $Z = 0.010$ ,  $Z = 0.014$ , and  $Z = 0.020$ , respectively. The cluster ages obtained by CG20 and by our ANN analysis are also shown as a reference, setting a constant uncertainty budget at 0.25 dex for the former. The errors on the period are negligible and therefore not included in the plots.

Cepheids in Galactic open clusters. We follow the Bayesian approach proposed by Anderson, Eyer, & Mowlavi (2013), focusing only on the relative position and kinematics of the Cepheid and its potential host.

After investigating more than 40,000 possible combinations (combos) selected by their on-sky projected distance, we found 67 with a probability of association larger than 10 per cent, including 44 with a posterior probability larger than 25 per cent. Additionally, we found 96 possible associations with probabilities between 1 and 10 per cent, mostly in newly discovered open clusters. Within the list of combos with probabilities  $> 0.01$  (163 in total), we report 19 that are consistent with previously known cluster Cepheids. Six literature combos are unlikely associations given their extremely small membership probabilities.

We advocate for dedicated follow-up studies including a detailed chemical investigation ("chemical tagging"; Freeman & Bland-Hawthorn 2002) and an accurate age determination. For combos with a membership probability higher than 10 per cent, logarithmic ages range from 6.42 (2.6 Myr) and 8.72 (525 Myr), with a median age of 7.80 (63 Myr), according to the age determinations of Cantat-Gaudin et al. (2020).

In an attempt to compare the age of Cepheids as given through isochrone fitting of the cluster population with the age given by theoretical period-age relations, we derived cluster ages using our own method and a publicly available code based on artificial neural networks. Despite an overall good agreement with literature values, we conclude that current age determinations for young open clusters do not reach the required accuracy ( $\log(t) < 0.2$ ) for the proposed goal. We argue that the reason is intrinsic to young open clusters, especially the less massive ones, due to the lack of MSTO stars. Such conclusions have already been reported by, e.g., Senchyna et al. (2015). We believe that upcoming Gaia data releases will allow us to over-

come this difficulty by providing colour-magnitude diagrams with extremely high levels of completeness and purity. Other approaches to possibly avoid some of these difficulties could come from the comparison of their observed and theoretical luminosity functions (see, e.g., Piskunov et al. 2004), or by complementing Gaia data by reddening-free indices and spectral types for upper main-sequence stars. We note in passing that Peña Ramírez et al. (2021) pre-selected potential cluster members via their Gaia DR2 proper motions using Gaussian mixture models, and assigned membership probabilities using the same unsupervised machine learning method (UPMASK) as in Cantat-Gaudin et al. (2018b) and Cantat-Gaudin & Anders (2020), but on near-infrared data instead of Gaia DR2 photometry. For the six clusters in their study, they report on average 45 per cent more cluster members than Cantat-Gaudin et al. (2018b) and Cantat-Gaudin & Anders (2020).

Despite a much larger number of clusters and Cepheids in the input catalogues, the number of high probability combos did not increase much. Even assuming that all cluster Cepheids pairs with  $P(A|B) > 0.01$  represent a true association, which is far from being realistic, we infer 4.1 per cent (121/2921)<sup>9</sup> as an upper limit to the fraction of classical Cepheids in open clusters. Anderson & Riess (2018), using the bona-fide cluster Cepheids described in A13, report an upper limit of 8.5 per cent for the clustered fraction of fundamental-mode Cepheids within 2 kpc from the Sun. Anderson & Riess (2018) also estimated the clustered fraction of fundamental-mode Cepheids in the Small and Large Magellanic Clouds to 6 and 11 per cent, respectively, and to 2.5 per cent in M31. Although the fraction presumably varies from galaxy to galaxy, even within a given galaxy, and also with time, these numbers all suggest a low fraction of Cepheids in clusters.

<sup>9</sup> For this, we also impose that a given Cepheid is associated with a unique cluster, therefore we consider 121 combos instead of 163.

Since very young ( $< 20$  Myr) clusters are overabundant, it is known that young clusters dissolve quickly, whether it is a consequence of gas expulsion or of their stellar dynamic and stellar evolution-driven expansion (e.g., Lada & Lada 2003; Goodwin & Bastian 2006; Moeckel et al. 2012), and these dissolutions can occur as fast as 100 Myr even for relatively massive clusters (of  $\sim 1,000 M_{\odot}$  Shukirgaliyev et al. 2018). In contrast, Cepheids have ages ranging from a few tens to a few hundred Myr (e.g., Anderson et al. 2016). The low fraction of Cepheids in clusters could then be related to the rapid dissolution of young clusters, or alternatively indicate that they are born elsewhere.

After estimating the age distribution of Galactic open clusters within a cylinder of 2 kpc radius from the Sun (taking into account age-dependent completeness limits), Anders et al. (2021) derived the star formation rate in clusters in the Solar vicinity, compared it to the total star formation rate in the solar vicinity (Mor et al. 2019), and concluded that only  $\sim 16$  per cent of stars formed in bound clusters. This result is in line with recent findings where star formation takes place at all scales and in unbound structures rather than in clusters (see e.g., Ward, Kruijssen, & Rix 2020, or the review by Adamo et al. 2020).

To better investigate the birthplace of Cepheids, one could envision adapting the prior (which currently only relies on the on-sky separation between clusters and Cepheids) to take into account the dynamical state of the cluster (its possible ongoing dissolution), in line with the findings of, e.g., Meingast, Alves, & Rottensteiner (2021). This could already provide higher membership probabilities for Cepheids about to leave a cluster, as it seems to be the case for QZ Nor as reported by Breuval et al. (2020), or those who just left it. An even more promising alternative would be to exploit conservative integrals of motion, as is done in the halo to identify globular cluster escapees and link them to their original cluster (see e.g., Hanke et al. 2020). Together with the aforementioned chemical tagging, this might render it possible to associate a given Cepheid and other nearby young stars with a unique birthplace, of any nature whatsoever.

## ACKNOWLEDGEMENTS

We thank the anonymous referee for her/his thorough feedback, which helped improve the quality of this manuscript. The results of this work were obtained using data from the European Space Agency (ESA) mission Gaia (<https://www.cosmos.esa.int/gaia>), processed by the Gaia Data Processing and Analysis Consortium (DPAC). Funding for the DPAC has been provided by national institutions, in particular the institutions participating in the Gaia Multilateral Agreement (MLA). G.M. acknowledges S. Yen and M. Hanke for fruitful discussions and insights regarding the data analysis used for this study. G.M. gratefully acknowledges the support of the Hector Fellow Academy. B.L. and E.K.G. acknowledge the Deutsche Forschungsgemeinschaft (DFG, German Research Foundation) – Project-ID 138713538 – SFB 881 (“The Milky Way System”, subprojects A05, B05). This research has made use of pandas (McKinney 2010), numpy (van der Walt, Colbert, & Varoquaux 2011), the Astropy library (Astropy Collaboration et al. 2013, 2018), and the software TOPCAT (Taylor 2005). This research has made use of the VizieR catalogue access tool, CDS, Strasbourg, France. The original description of the VizieR service was published in A&AS 143, 23. The figures in this paper were produced with Matplotlib (Hunter 2007).

## DATA AVAILABILITY

The data underlying this article are publicly available and their sources are described in detail in this document. Tables containing the results of this study are provided as online supplementary material.

## REFERENCES

- Abolfathi B., et al., 2018, *ApJS*, 235, 42  
 Adamo A., et al., 2020, *SSRv*, 216, 69  
 An D., Terndrup D. M., Pinsonneault M. H., 2007, *ApJ*, 671, 1640  
 Anders F., Cantat-Gaudin T., Quadrino-Lodoso I., Gieles M., Jordi C., Castro-Ginard A., Balaguer-Núñez L., 2021, *A&A*, 645, L2. doi:10.1051/0004-6361/202038532  
 Anderson R. I., Eyer L., Mowlavi N., 2013, *MNRAS*, 434, 2238  
 Anderson R. I., Ekström S., Georgy C., Meynet G., Mowlavi N., Eyer L., 2014, *A&A*, 564, A100  
 Anderson R. I., Saio H., Ekström S., Georgy C., Meynet G., 2016, *A&A*, 591, A8  
 Anderson R. I., Riess A. G., 2018, *ApJ*, 861, 36. doi:10.3847/1538-4357/aac5e2  
 Astropy Collaboration, et al., 2013, *A&A*, 558, A33  
 Astropy Collaboration, et al., 2018, *AJ*, 156, 123  
 Baumgardt H., Dettbarn C., Wielen R., 2000, *A&AS*, 146, 251  
 Beccari G., Boffin H. M. J., Jerabkova T., 2020, *MNRAS*, 491, 2205. doi:10.1093/mnras/stz3195  
 Benedict G. F., et al., 2007, *AJ*, 133, 1810. doi:10.1086/511980  
 Bono G., Castellani V., Marconi M., 2000, *ApJ*, 529, 293  
 Bono G., Caputo F., Cassisi S., Marconi M., Piersanti L., Tornambè A., 2000, *ApJ*, 543, 955  
 Bono G., Marconi M., Cassisi S., Caputo F., Gieren W., Pietrzynski G., 2005, *ApJ*, 621, 966  
 Boubert D., Everall A., 2020, *MNRAS*, 497, 4246  
 Bossini D., et al., 2019, *A&A*, 623, A108  
 Bressan A., Marigo P., Girardi L., Salasnich B., Dal Cero C., Rubele S., Nanni A., 2012, *MNRAS*, 427, 127  
 Breuval L., et al., 2020, *A&A*, 643, A115. doi:10.1051/0004-6361/202038633  
 Buder S., et al., 2018, *MNRAS*, 478, 4513  
 Cantat-Gaudin T., Anders F., 2020, *A&A*, 633, A99  
 Cantat-Gaudin T., et al., 2018a, *A&A*, 615, A49  
 Cantat-Gaudin T., et al., 2018b, *A&A*, 618, A93  
 Cantat-Gaudin T., et al., 2019, *A&A*, 624, A126  
 Cantat-Gaudin T., et al., 2020, *A&A*, 640, A1  
 Cantat-Gaudin T., Brandt T. D., 2021, *arXiv*, arXiv:2103.07432  
 Cardelli J. A., Clayton G. C., Mathis J. S., 1989, *ApJ*, 345, 245  
 Carrera R., et al., 2019, *A&A*, 623, A80  
 Castro-Ginard A., Jordi C., Luri X., Julbe F., Morvan M., Balaguer-Núñez L., Cantat-Gaudin T., 2018, *A&A*, 618, A59  
 Castro-Ginard A., Jordi C., Luri X., Cantat-Gaudin T., Balaguer-Núñez L., 2019, *A&A*, 627, A35  
 Castro-Ginard A., et al., 2020, *A&A*, 635, A45  
 Chabrier G., 2001, *ApJ*, 554, 1274  
 Chen X., de Grijs R., Deng L., 2015, *MNRAS*, 446, 1268  
 Chen X., Wang S., Deng L., de Grijs R., Yang M., 2018, *ApJS*, 237, 28. doi:10.3847/1538-4365/aad32b  
 Choi J., Dotter A., Conroy C., Cantiello M., Paxton B., Johnson B. D., 2016, *ApJ*, 823, 102  
 Claria J. J., Lapasset E., Bosio M. A., 1991, *MNRAS*, 249, 193. doi:10.1093/mnras/249.2.193  
 Clark J. S., Negueruela I., Lohr M. E., Dorda R., González-Fernández C., Lewis F., Roche P., 2015, *A&A*, 584, L12. doi:10.1051/0004-6361/201527360  
 Clementini G., et al., 2019, *A&A*, 622, A60  
 Coulson I. M., Caldwell J. A. R., 1985, *MNRAS*, 216, 671

- Czekaj M. A., Robin A. C., Figueras F., Luri X., Haywood M., 2014, *A&A*, 564, A102
- De Somma G., Marconi M., Molinaro R., Cignoni M., Musella I., Ripepi V., 2020, *ApJS*, 247, 30. doi:10.3847/1538-4365/ab7204
- De Somma G., Marconi M., Cassisi S., Ripepi V., Leccia S., Molinaro R., Musella I., 2020, *MNRAS*, 496, 5039
- Dékány I., Hajdu G., Grebel E. K., Catelan M., 2019, *ApJ*, 883, 58. doi:10.3847/1538-4357/ab3b60
- Dias W. S., Alessi B. S., Moitinho A., Lépine J. R. D., 2002, *A&A*, 389, 871
- Dias W. S., Monteiro H., Caetano T. C., Oliveira A. F., 2012, *A&A*, 539, A125. doi:10.1051/0004-6361/201118206
- Donor J., et al., 2020, *AJ*, 159, 199
- Dotter A., 2016, *ApJS*, 222, 8
- Efremov, Y. N. 1964, *Peremennye Zvezdy*, 15, 242
- Efremov I. N., 1978, *SvA*, 22, 161
- Efremov Y. N., 2003, *ARep*, 47, 1000
- Eggen O. J., 1980, *IBVS*, 1853, 1
- Eldridge J. J., 2012, *MNRAS*, 422, 794
- ESA, 1997, *ESA Special Publication*, 1200
- Evans D. W., et al., 2018, *A&A*, 616, A4
- Fabricius C., et al., 2020, *arXiv*, arXiv:2012.06242
- Feast M. W., 1957, *MNRAS*, 117, 193
- Ferreira F. A., Santos J. F. C., Corradi W. J. B., Maia F. F. S., Angelo M. S., 2019, *MNRAS*, 483, 5508
- Ferreira F. A., Corradi W. J. B., Maia F. F. S., Angelo M. S., Santos J. F. C., 2020, *MNRAS*, 496, 2021
- Ferreira Lopes C. E., et al., 2020, *MNRAS*, 496, 1730. doi:10.1093/mnras/staa1352
- Ferreira F. A., Corradi W. J. B., Maia F. F. S., Angelo M. S., Santos J. F. C., 2021, *MNRAS*, 502, L90. doi:10.1093/mnras/slab011
- Flower P. J., 1978, *ApJ*, 224, 948. doi:10.1086/156443
- Fouesneau M., Lançon A., 2010, *A&A*, 521, A22
- Freeman K., Bland-Hawthorn J., 2002, *ARA&A*, 40, 487. doi:10.1146/annurev.astro.40.060401.093840
- Froebrich D., Scholz A., Raftery C. L., 2007, *MNRAS*, 374, 399. doi:10.1111/j.1365-2966.2006.11148.x
- Fry A. M., Carney B. W., 1997, *AJ*, 113, 1073. doi:10.1086/118324
- Gaia Collaboration, et al., 2016, *A&A*, 595, A1
- Gaia Collaboration, et al., 2018, *A&A*, 616, A1
- Gaia Collaboration, Brown A. G. A., Vallenari A., Prusti T., de Bruijne J. H. J., Babusiaux C., Biermann M., 2020, *arXiv*, arXiv:2012.01533
- Genovali K., et al., 2015, *A&A*, 580, A17. doi:10.1051/0004-6361/201525894
- Glatt K., Grebel E. K., Koch A., 2010, *A&A*, 517, A50. doi:10.1051/0004-6361/201014187
- Goodwin S. P., Bastian N., 2006, *MNRAS*, 373, 752. doi:10.1111/j.1365-2966.2006.11078.x
- Grebel E. K., Brandner W., 1998, in Richtler T., Braun J. M., eds, *Magellanic Clouds and Other Dwarf Galaxies*. Shaker Verlag, Aachen, p. 151
- Hanke M., Koch A., Prudil Z., Grebel E. K., Bastian U., 2020, *A&A*, 637, A98
- Heinze A. N., et al., 2018, *AJ*, 156, 241. doi:10.3847/1538-3881/aae47f
- Hidalgo S. L., et al., 2018, *ApJ*, 856, 125. doi:10.3847/1538-4357/aab158
- Holtzman J. A., et al., 2018, *AJ*, 156, 125. doi:10.3847/1538-3881/aad4f9
- Hoyle F., Shanks T., Tanvir N. R., 2003, *MNRAS*, 345, 269
- Hunt E. L., Reffert S., 2021, *A&A*, 646, A104. doi:10.1051/0004-6361/202039341
- Hunter, J. D. 2007, *Computing in Science and Engineering*, 9, 90
- Inno L., et al., 2015, in Points S., Kunder A., eds, *The Recent Star Formation History of the Magellanic Clouds Traced by Classical Cepheids*, Vol. 491, *Astronomical Society of the Pacific Conference Series*. p. 265
- Irwin J. B., 1955, *MNSSA*, 14, 38
- Jayasinghe T., et al., 2018, *MNRAS*, 477, 3145. doi:10.1093/mnras/sty838
- Jayasinghe T., et al., 2019a, *MNRAS*, 486, 1907. doi:10.1093/mnras/stz844
- Jayasinghe T., et al., 2019b, *MNRAS*, 485, 961. doi:10.1093/mnras/stz444
- Jaynes E. T. 2003, *Probability Theory - The Logic of Science*. Cambridge Univ. Press, Cambridge
- Jönsson H., et al., 2020, *AJ*, 160, 120. doi:10.3847/1538-3881/aba592
- Kervella P., et al., 2019, *A&A*, 623, A116
- Kharchenko N. V., Piskunov A. E., Röser S., Schilbach E., Scholz R.-D., 2005, *A&A*, 438, 1163
- Kharchenko N. V., Piskunov A. E., Röser S., Schilbach E., Scholz R.-D., 2005, *A&A*, 440, 403
- Kharchenko N. V., Piskunov A. E., Schilbach E., Röser S., Scholz R.-D., 2012, *A&A*, 543, A156
- Kharchenko N. V., Piskunov A. E., Schilbach E., Röser S., Scholz R.-D., 2013, *A&A*, 558, A53
- Kholopov P. N., 1956, *Peremennye Zvezdy*, 11, 325
- Kippenhahn R., Smith L., 1969, *A&A*, 1, 142
- Kounkel M., Covey K., Stassun K. G., 2020, *AJ*, 160, 279. doi:10.3847/1538-3881/abc0e6
- Kraft R. P., 1962, *IAUTB*, 11B, 298
- Kukarkin B. V., et al., 1969, *General Catalogue of Variable Stars. Volume 1. Constellations Andromeda – Grus*
- Lada C. J., Lada E. A., 2003, *ARA&A*, 41, 57. doi:10.1146/annurev.astro.41.011802.094844
- Leavitt H. S., Pickering E. C., 1912, *Harvard College Observatory Circular*, 173
- Lemasle B., et al., 2008, *A&A*, 490, 613. doi:10.1051/0004-6361:200810192
- Lemasle B., et al., 2017, *A&A*, 608, A85
- Lindgren L., et al., 2018, *A&A*, 616, A2
- Lindgren L., Bastian U., Biermann M., Bombrun A., de Torres A., Gerlach E., Geyer R., et al., 2020, *arXiv*, arXiv:2012.01742
- Liu L., Pang X., 2019, *ApJS*, 245, 32
- Lohr M. E., Negueruela I., Taberner H. M., Clark J. S., Lewis F., Roche P., 2018, *MNRAS*, 478, 3825
- Lyngå G., Lindgren L., 1998, *NewA*, 3, 121
- Madore B. F., Freedman W. L., 1991, *PASP*, 103, 933
- Magnier E. A., Auguestijn T., Prins S., van Paradijs J., Lewin W. H. G., 1997a, *A&AS*, 126, 401
- Magnier E. A., Prins S., Auguestijn T., van Paradijs J., Lewin W. H. G., 1997b, *A&A*, 326, 442
- Magrini L., et al., 2017, *A&A*, 603, A2. doi:10.1051/0004-6361/201630294
- Mahalanobis P. C. 1936, *On the generalised distance in statistics*, *Proceedings of the National Institute of Sciences of India*, 2, 49–55
- Majaess D. J., Turner D. G., Lane D. J., 2008, *MNRAS*, 390, 1539
- Majaess D., et al., 2011, *ApJL*, 741, L27. doi:10.1088/2041-8205/741/2/L27
- Majaess D., et al., 2013a, *Ap&SS*, 347, 61
- Majaess D., et al., 2013b, *A&A*, 560, A22
- Mateo M., Madore B., 1988, *ASPC*, 4, 174
- Matthews J. M., Gieren W. P., Mermilliod J.-C., Welch D. L., 1995, *AJ*, 110, 2280
- McKinney W., 2010, in van der Walt S. & Millman J., eds, *Proceedings of the 9th Python in Science Conference*, 56 - 61
- Meingast S., Alves J., Rottensteiner A., 2021, *A&A*, 645, A84. doi:10.1051/0004-6361/202038610
- Mel'nik A. M., Rautiainen P., Berdnikov L. N., Dambis A. K., Rastorguev A. S., 2015, *AN*, 336, 70
- Mermilliod J. C., 1988, *Bulletin d'Information du Centre de Données Stellaires*, 35, 77
- Meyer-Hofmeister E., 1969, *A&A*, 2, 143
- Moeckel N., Holland C., Clarke C. J., Bonnell I. A., 2012, *MNRAS*, 425, 450. doi:10.1111/j.1365-2966.2012.21494.x
- Monteiro H., Dias W. S., Caetano T. C., 2010, *A&A*, 516, A2. doi:10.1051/0004-6361/200913677
- Mor R., Robin A. C., Figueras F., Roca-Fàbrega S., Luri X., 2019, *A&A*, 624, L1. doi:10.1051/0004-6361/201935105
- Mucciarelli A., et al., 2011, *MNRAS*, 413, 837. doi:10.1111/j.1365-2966.2010.18167.x
- Musella I., et al., 2016, *MNRAS*, 457, 3084. doi:10.1093/mnras/stw151
- Negueruela I., Monguió M., Marco A., Taberner H. M., González-Fernández C., Dorda R., 2018, *MNRAS*, 477, 2976. doi:10.1093/mnras/sty718
- Negueruela I., Dorda R., Marco A., 2020, *MNRAS*, 494, 3028
- Netopil M., Paurzen E., Heiter U., Soubiran C., 2016, *A&A*, 585, A150. doi:10.1051/0004-6361/201526370



- Pang X., Li Y., Tang S.-Y., Pasquato M., Kouwenhoven M. B. N., 2020, *ApJL*, 900, L4. doi:10.3847/2041-8213/abad28
- Paxton B., Bildsten L., Dotter A., Herwig F., Lesaffre P., Timmes F., 2011, *ApJS*, 192, 3
- Paxton B., et al., 2013, *ApJS*, 208, 4
- Payne-Gaposchkin C. H., 1974, *SCoA*, 16
- Pel J. W., 1985, *IAU Colloq. 82: Cepheids: Theory and Observation*, 1
- Peña Ramírez K., González-Fernández C., Chené A.-N., Ramírez Alegría S., 2021, *MNRAS*, 503, 1864. doi:10.1093/mnras/stab328
- Pietrzyński G., Gieren W., Fouqué P., Pont F., 2002, *AJ*, 123, 789
- Piskunov A. E., Belikov A. N., Kharchenko N. V., Sagar R., Subramaniam A., 2004, *MNRAS*, 349, 1449
- Pojmanski G., Maciejewski G., 2004, *AcA*, 54, 153
- Popescu B., Hanson M. M., 2010, *ApJ*, 724, 296
- Prudil Z., Hanke M., Lemasle B., Crestani J., Braga V. F., Fabrizio M., Koch-Hansen A. J., et al., 2021, arXiv, arXiv:2102.01090
- Riess A. G., et al., 2018, *ApJ*, 855, 136
- Robichon N., Arenou F., Merrell J.-C., Turon C., 1999, *A&A*, 345, 471
- Romaniello M., et al., 2008, *A&A*, 488, 731. doi:10.1051/0004-6361:20065661
- Ripepi V., Molinaro R., Musella I., Marconi M., Leccia S., Eyer L., 2019, *A&A*, 625, A14
- Robin A. C., Reylé C., Derrière S., Picaud S., 2003, *A&A*, 409, 523
- Robin A. C., Reylé C., Fliri J., Czekaj M., Robert C. P., Martins A. M. M., 2014, *A&A*, 569, A13
- Robinson E., von Hippel T., Stein N., Stenning D., Wagner-Kaiser R., Si S., van Dyk D., 2016, *ascl.soft. ascl:1608.007*
- Roeser S., Demleitner M., Schilbach E., 2010, *AJ*, 139, 2440
- Röck, B., 2012, Master thesis, Univ. Heidelberg
- Röser S., Kharchenko N. V., Piskunov A. E., Schilbach E., Scholz R.-D., Zinnecker H., 2010, *AN*, 331, 519
- Salpeter E. E., 1955, *ApJ*, 121, 161
- Samus' N. N., Kazarovets E. V., Durlevich O. V., Kireeva N. N., Pastukhova E. N., 2017, *ARep*, 61, 80
- Sánchez N., Alfaro E. J., López-Martínez F., 2020, *MNRAS*, 495, 2882
- Sandage A., 1958, *ApJ*, 128, 150
- Schmidt E. G., 1982, *AJ*, 87, 1197. doi:10.1086/113201
- Schultz G. V., Wiemer W., 1975, *A&A*, 43, 133
- Senchyna P., et al., 2015, *ApJ*, 813, 31. doi:10.1088/0004-637X/813/1/31
- Shukirgaliyev B., Parmentier G., Just A., Berczik P., 2018, *ApJ*, 863, 171
- Sim G., Lee S. H., Ann H. B., Kim S., 2019, *JKAS*, 52, 145
- Skowron D. M., et al., 2019a, *Sci*, 365, 478. doi:10.1126/science.aau3181
- Skowron D. M., et al., 2019b, *AcA*, 69, 305. doi:10.32023/0001-5237/69.4.1
- Soszyński I., et al., 2017, *AcA*, 67, 297. doi:10.32023/0001-5237/67.4.1
- Soszyński I., et al., 2020, *AcA*, 70, 101. doi:10.32023/0001-5237/70.2.2
- Storm J., et al., 2011, *A&A*, 534, A94. doi:10.1051/0004-6361/201117155
- Tammann G. A., 1970, *IAUS*, 38, 236
- Taylor M. B., 2005, in Shopbell P., Britton M., Ebert R., eds, *ASP Conf. Ser. Vol. 347, Astronomical Data Analysis Software and Systems XIV*. Astron. Soc. Pac., San Francisco, p. 29
- Tian H.-J., 2020, *ApJ*, 904, 196. doi:10.3847/1538-4357/abbf4b
- Torrealba G., Belokurov V., Koposov S. E., 2019, *MNRAS*, 484, 2181
- Tsarevsky G. S., Ureche V., Efremov Y. N., 1966, *ATsir*, 367
- Turner D. G., 1976, *AJ*, 81, 1125. doi:10.1086/111994
- Turner D. G., 1977, *PASP*, 89, 277. doi:10.1086/130117
- Turner D. G., 1980, *ApJ*, 240, 137
- Turner D. G., 1981, *AJ*, 86, 231. doi:10.1086/112878
- Turner D. G., 1982, *PASP*, 94, 1003. doi:10.1086/131100
- Turner D. G., 1984, *JRASC*, 78, 229
- Turner D. G., Pedreros M., 1985, *AJ*, 90, 1231. doi:10.1086/113830
- Turner D. G., 1986, *AJ*, 92, 111
- Turner D. G., Forbes D., Pedreros M., 1992, *AJ*, 104, 1132
- Turner D. G., van den Bergh S., Younger P. F., Danks T. A., Forbes D., 1993, *ApJS*, 85, 119. doi:10.1086/191756
- Turner D. G., 1998a, *AJ*, 116, 274
- Turner D. G., Ibrahimov M. A., Mandushev G. I., Berdnikov L. N., Horsford A. J., 1998b, *JRASC*, 92, 145
- Turner D. G., Pedreros M. H., Walker A. R., 1998c, *AJ*, 115, 1958. doi:10.1086/300316
- Turner D. G., Burke J. F., 2002, *AJ*, 124, 2931
- Turner D. G., Forbes D., van den Bergh S., Younger P. F., Berdnikov L. N., 2005, *AJ*, 130, 1194
- Turner D. G., et al., 2008, *MNRAS*, 388, 444
- Turner D. G., 2010, *Ap&SS*, 326, 219
- Turner D. G., van den Bergh S., Younger P. F., Majaess D. J., Pedreros M. H., Berdnikov L. N., 2012, *AJ*, 144, 187. doi:10.1088/0004-6256/144/6/187
- Udalski A., Szymański M. K., Szymański G., 2015, *AcA*, 65, 1
- Udalski A., et al., 2018, *AcA*, 68, 315
- Usenko I. A., Kniazev A. Y., Katkov I. Y., Kovtyukh V. V., Mishenina T. V., Miroshnichenko A. S., Turner D. G., 2019, *OAP*, 32, 91
- van den Bergh S., 1957, *ApJ*, 126, 323
- van der Walt S., Colbert S. C., Varoquaux G., 2011, *Computing in Science and Engineering*, 13, 22. doi:10.1109/MCSE.2011.37
- van Leeuwen F., 2007, *Hipparcos, the New Reduction of the Raw Data: Astrophysics and Space Science Library, Vol. 350*, Springer Science+Business Media B.V., Berlin. doi:10.1007/978-1-4020-6342-8
- Vasiliev E., 2019, *MNRAS*, 489, 623. doi:10.1093/mnras/stz2100
- von Hippel T., Jefferys W. H., Scott J., Stein N., Winget D. E., De Gennaro S., Dam A., et al., 2006, *ApJ*, 645, 1436. doi:10.1086/504369
- Walker A. R., 1985a, *MNRAS*, 213, 889. doi:10.1093/mnras/213.4.889
- Walker A. R., 1985b, *MNRAS*, 214, 45
- Walker A. R., 1987, *MNRAS*, 229, 31. doi:10.1093/mnras/229.1.31
- Wang S., Chen X., de Grijs R., Deng L., 2018, *ApJ*, 852, 78
- Ward J. L., Kruijssen J. M. D., Rix H.-W., 2020, *MNRAS*, 495, 663
- Watson C. L., Henden A. A., Price A., 2006, *SASS*, 25, 47
- Watson C., Henden A. A., Price A., 2014, *yCat, B/vsx*
- Weidner C., Kroupa P., 2006, *MNRAS*, 365, 1333
- Yilmaz F., 1966, *ZA*, 64, 54
- Zinnecker H., Piskunov A. E., Kharchenko N. V., Röser S., Schilbach E., Scholz R.-D., 2009, *IAUS*, 254, 221

Table A1: Cluster - Cepheid pairs with membership probabilities  $P(A|B)$  between 0.01 and 0.10. The table lists the cluster names as well as their MWSC identification in the K13 catalogue, the Cepheid names, the angular separation of the pair over the cluster's  $r_1$  ( $Sep/r_1$ ), the list of constraints used to derive the membership probability, the prior  $P(A)$ , the likelihood  $P(A|B)$  and the membership probability  $P(B|A)$ . The full table is provided as supplementary material.

Open cluster	MWSC ID	Cepheid	Sep/ $r_1$	Constraints	$P(A)$	$P(B A)$	$P(A B)$
UFMG 54	–	OGLE-GD-CEP-0964	11.56	$\varpi, \mu_\alpha^*, \mu_\delta$	0.10	1.00	0.10
NGC 6664	2962	EV Sct	3.64	$\varpi, V_r, \mu_\alpha^*, \mu_\delta$	0.12	0.80	0.10
LP 888	–	CG Cas	2.69	$\varpi, \mu_\alpha^*, \mu_\delta$	0.27	0.35	0.09
LP 58	–	AM Vel	4.09	$\varpi, \mu_\alpha^*, \mu_\delta$	0.09	1.00	0.09
BH 99	1831	OGLE-GD-CEP-1669	1.68	$\varpi, \mu_\alpha^*, \mu_\delta$	0.58	0.16	0.09
Platais 8	1629	OGLE-GD-CEP-0507	3.59	$\varpi, \mu_\alpha^*, \mu_\delta$	0.13	0.66	0.09
UBC 135	–	GI Cyg	0.98	$\varpi, \mu_\alpha^*, \mu_\delta$	1.00	0.08	0.08
Collinder 228	1845	GDS J1046447-601605	2.76	$\varpi, \mu_\alpha^*, \mu_\delta$	0.26	0.32	0.08
Loden 1409	2249	OGLE-GD-CEP-0998	3.46	$\varpi, \mu_\alpha^*, \mu_\delta$	0.10	0.81	0.08
NGC 5662	2234	V Cen	1.51	$\varpi, V_r, \mu_\alpha^*, \mu_\delta$	0.67	0.12	0.08

\* Uncertain Cepheid classification, as noted by the OGLE team.

† Coincidence with a cluster in the catalogues of [Liu & Pang \(2019\)](#) or [Sim et al. \(2019\)](#), according to [Castro-Ginard et al. \(2020\)](#).

**Table A2.** Prior, likelihood and membership probability for literature combos. We list the cluster and Cepheid names, their angular separation as a function of  $r_1$ , and the constraints used in the analysis. For the combos in the top list, which appear at least once in Turner’s database (only potential combos with open clusters), A13 (with  $P(A|B) > 0.10$ , from that work), or Chen, de Grijs, & Deng (2015), we obtain membership probabilities  $> 1$  per cent. We included in this list the cluster Cepheids recently confirmed by Clark et al. (2015), Lohr et al. (2018), and Negueruela, Dorda, & Marco (2020), as we considered them in the combo descriptions presented in Section 5. Combos in the bottom part of this table are those considered missed, and are listed as true associations in at least three of the aforementioned catalogues plus Röck (2012). In the last column we list references where the Cepheid membership to the cluster is discussed: a : Lohr et al. (2018), b : Negueruela et al. (2018), c : Anderson, Eyer, & Mowlavi (2013), d : Walker (1985a), e : An, Terndrup, & Pinsonneault (2007), f : Turner (2010), g : Majaess et al. (2011), h : Chen, de Grijs, & Deng (2015), i : Sandage (1958), j : Mateo & Madore (1988), k : Matthews et al. (1995), l : Irwin (1955), m : Kholopov (1956), n : Feast (1957), o : Pel (1985), p : Turner, Forbes, & Pedreros (1992), q : Turner, Pedreros, & Walker (1998c), r : Coulson & Caldwell (1985), s : Walker (1985b), t : Hoyle, Shanks, & Tanvir (2003), u : Clark et al. (2015), v : Flower (1978), w : Turner (1981), x : Negueruela, Dorda, & Marco (2020), y : Turner (1986), z : Walker (1987),  $\alpha$  : Turner (1976),  $\beta$  : Schmidt (1982),  $\gamma$  : Turner & Burke (2002),  $\delta$  : Turner (1982),  $\epsilon$  : Claria, Lapasset, & Bosio (1991),  $\zeta$  : Turner et al. (2008),  $\eta$  : Turner & Pedreros (1985),  $\theta$  : Turner (1998a),  $\iota$  : Yilmaz (1966),  $\kappa$  : Turner (1980),  $\lambda$  : Turner et al. (1993),  $\lambda$  : Turner et al. (1998b).

Bona fide combos recovered							
Open cluster	Cepheid	Sep/ $r_1$	Constraints	$P(A)$	$P(B A)$	$P(A B)$	References
Berkeley 55	ASASSN-V J211659.90+514558.7	0.29	$\varpi, \mu_\alpha^*, \mu_\delta$	1.00	0.94	0.94	a
Berkeley 51	ASASSN-V J201151.18+342447.2	0.75	$\varpi, \mu_\alpha^*, \mu_\delta$	1.00	0.85	0.85	a, b
Lynga 6	TW Nor	0.39	$\varpi, V_r, \mu_\alpha^*, \mu_\delta$	1.00	0.82	0.82	c, d, e, f, g
NGC 7790	CF Cas	0.30	$\varpi, V_r, \mu_\alpha^*, \mu_\delta$	1.00	0.80	0.80	c, h, i, j, k
IC 4725	U Sgr	0.10	$\varpi, V_r, \mu_\alpha^*, \mu_\delta$	1.00	0.75	0.75	c, e, h, l, m, n, o
NGC 129	DL Cas	0.04	$\varpi, V_r, \mu_\alpha^*, \mu_\delta$	1.00	0.75	0.75	c, h, m, p
vdBergh 1	CV Mon	0.68	$\varpi, \mu_\alpha^*, \mu_\delta$	1.00	0.67	0.67	c, h, q
NGC 6067	V0340 Nor	0.20	$\varpi, \mu_\alpha^*, \mu_\delta$	1.00	0.66	0.66	c, e, f, r, s, t
BH 222	OGLE-BLG-CEP-110	0.41	$\varpi, \mu_\alpha^*, \mu_\delta$	1.00	0.65	0.65	a, u
NGC 6649	V0367 Set	0.73	$\varpi, \mu_\alpha^*, \mu_\delta$	1.00	0.63	0.63	c, v, w
UBC 130	SV Vul	1.41	$\varpi, \mu_\alpha^*, \mu_\delta$	0.73	0.71	0.52	x
NGC 7790	CE Cas B	0.51	$\varpi, \mu_\alpha^*, \mu_\delta$	1.00	0.50	0.50	c, h, i, j, k
FSR 0158	GQ Vul	1.80	$\varpi, \mu_\alpha^*, \mu_\delta$	0.53	0.89	0.47	c
NGC 6087	S Nor	0.14	$\varpi, V_r, \mu_\alpha^*, \mu_\delta$	1.00	0.38	0.38	c, h, l, m, n, y
NGC 7790	CE Cas A	0.50	$\varpi, \mu_\alpha^*, \mu_\delta$	1.00	0.28	0.28	c, h, i, j, k
Ruprecht 79	CS Vel	0.84	$\varpi, V_r, \mu_\alpha^*, \mu_\delta$	1.00	0.23	0.23	f, z
NGC 6664	EV Set	3.64	$\varpi, V_r, \mu_\alpha^*, \mu_\delta$	0.12	0.80	0.10	$\alpha, \beta, \gamma$
NGC 5662	V Cen	1.51	$\varpi, V_r, \mu_\alpha^*, \mu_\delta$	0.67	0.12	0.08	e, f, h, $\delta, \epsilon$
ASCC 69	S Mus	4.66	$\varpi, V_r, \mu_\alpha^*, \mu_\delta$	0.06	0.58	0.03	c, h

Missed							
Open cluster	Cepheid	Sep/ $r_1$	Constraints	$P(A)$	$P(B A)$	$P(A B)$	References
Berkeley 58	CG Cas	1.60	$\varpi, V_r, \mu_\alpha^*, \mu_\delta$	0.62	0.00	0.00	h, $\zeta$
Collinder 394	BB Sgr	1.59	$\varpi, V_r, \mu_\alpha^*, \mu_\delta$	0.63	0.00	0.00	c, f, h, $\eta$
Ruprecht 175	X Cyg	7.52	$\varpi, \mu_\alpha^*, \mu_\delta$	0.00	0.00	0.00	h, $\theta$
Trumpler 35	RU Set	5.12	$\varpi, V_r, \mu_\alpha^*, \mu_\delta$	0.04	0.00	0.00	c, f, s, $\iota, \kappa$
Turner 2	WZ Sgr	2.56	$\varpi, \mu_\alpha^*, \mu_\delta$	0.21	0.00	0.00	c, h, $\iota$
Turner 9	SU Cyg	0.01	$\varpi, V_r, \mu_\alpha^*, \mu_\delta$	1.00	0.00	0.00	c, f, $\lambda$
Berkeley 58	CG Cas	1.60	$\varpi, V_r, \mu_\alpha^*, \mu_\delta$	0.62	0.00	0.00	h, $\zeta$
Collinder 394	BB Sgr	1.59	$\varpi, V_r, \mu_\alpha^*, \mu_\delta$	0.63	0.00	0.00	c, f, h, $\eta$
Ruprecht 175	X Cyg	7.52	$\varpi, \mu_\alpha^*, \mu_\delta$	0.00	0.00	0.00	h, $\theta$
Trumpler 35	RU Set	5.12	$\varpi, V_r, \mu_\alpha^*, \mu_\delta$	0.04	0.00	0.00	c, f, t, $\iota, \kappa$
Turner 2	WZ Sgr	2.56	$\varpi, \mu_\alpha^*, \mu_\delta$	0.21	0.00	0.00	c, h, $\iota$
Turner 9	SU Cyg	0.01	$\varpi, V_r, \mu_\alpha^*, \mu_\delta$	1.00	0.00	0.00	c, f, $\lambda$

Table A3: Same as Table A1 for combos Cluster - Cepheid pairs with low priors  $P(A)$ , but high likelihood ( $P(B|A) > 0.85$ ). The full table is provided as supplementary material.

Open cluster	MWSC ID	Cepheid	Sep/ $r_1$	Constraints	$P(B A)$
ASCC 59	1793	OGLE-GD-CEP-0507	7.38	$\varpi, \mu_\alpha^*, \mu_\delta$	0.99
ASCC 60	1823	OGLE-GD-CEP-0507	12.12	$\varpi, \mu_\alpha^*, \mu_\delta$	0.86
Alessi 18	1284	BE Pup	51.21	$\varpi, \mu_\alpha^*, \mu_\delta$	0.90
BH 118	1939	OGLE-GD-CEP-0633	76.23	$\varpi, \mu_\alpha^*, \mu_\delta$	0.87
BH 144	2098	OGLE-GD-CEP-0869	49.27	$\varpi, \mu_\alpha^*, \mu_\delta$	1.00
BH 144	2098	OGLE-GD-CEP-0873	50.10	$\varpi, \mu_\alpha^*, \mu_\delta$	0.98
BH 144	2098	GDS J1313507-642626	61.72	$\varpi, \mu_\alpha^*, \mu_\delta$	0.94
BH 151	2147	WISE J132924.6-625511	215.66	$\varpi, \mu_\alpha^*, \mu_\delta$	0.85
BH 222	2564	OGLE-BLG-CEP-173	85.59	$\varpi, \mu_\alpha^*, \mu_\delta$	0.93
BH 63	1653	OGLE-GD-CEP-0328	23.97	$\varpi, \mu_\alpha^*, \mu_\delta$	0.99

<sup>k</sup> Cluster with position and proper motion compatible with a cluster in K13, based on [Castro-Ginard et al. \(2020\)](#).



This paper has been typeset from a  $\text{\TeX}/\text{\LaTeX}$  file prepared by the author.

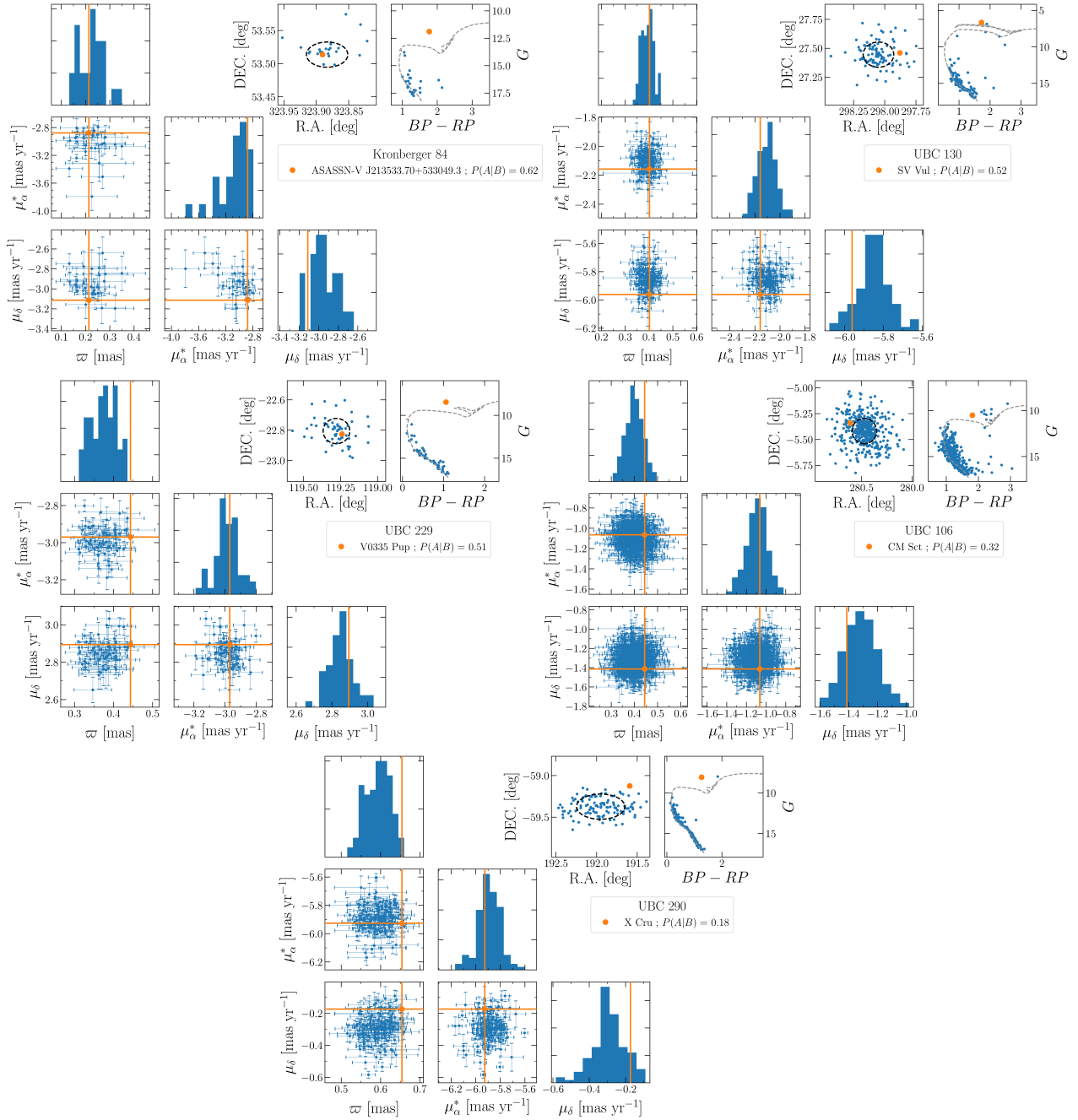


**Figure A1.** Distribution of the Gaia-based astrometry (parallaxes, proper motions, and positions) and colour-magnitude diagrams for the combos described in Section 5.4, for which a list of cluster members is provided by CG20. The information of the members (from CG20) is represented in blue, while the Cepheids properties are shown in orange. In the panels displaying the equatorial coordinates of the members, a black dashed line represent the clusters'  $r_1$ . PARSEC isochrones of solar metallicity are plotted in the colour-magnitude diagrams with grey dashed lines using the values derived by CG20 as a reference.

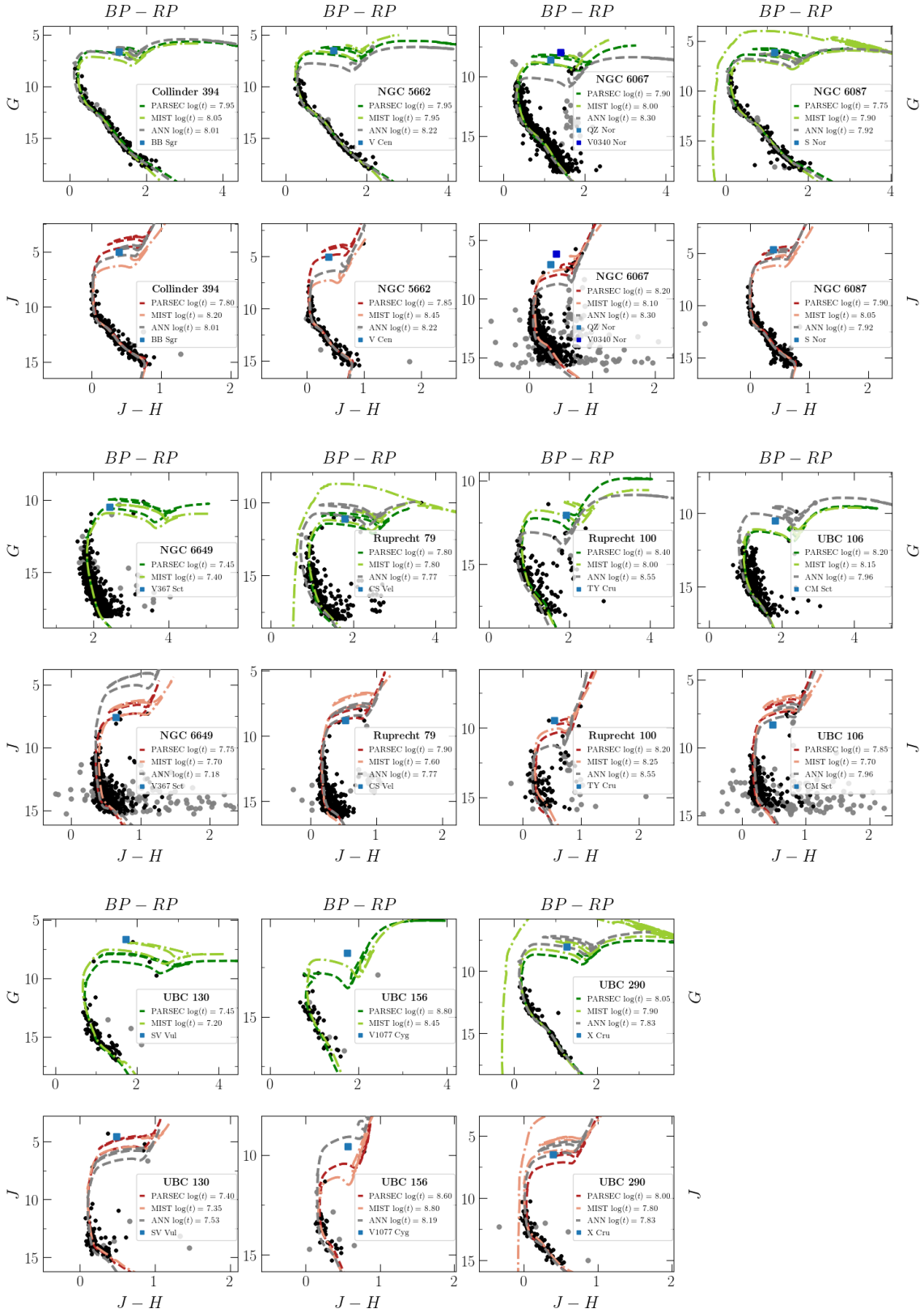


**Figure A2.** Colour-magnitude diagrams of the clusters studied in Section 6, with isochrones representing the results of Section 6.1. Cluster members from CG18b are shown with grey circles, whereas those used for the best-model determination are displayed in black. The outcomes of the ANN are plotted with PARSEC isochrones assuming solar metallicity (in grey), with the exception of the clusters marked as highly reddened in Table 2 (for the Gaia passband panels).